Construction and Building Materials 352 (2022) 128982

Contents lists available at ScienceDirect

Construction and Building Materials

journal homepage: www.elsevier.com/locate/conbuildmat

On the interaction between proteins and cracked cementitious surface

Elvis Baffoe, Ali Ghahremaninezhad *

Department of Civil, Architectural and Environmental Engineering, University of Miami, Coral Gables, FL 33146, United States

ARTICLE INFO

Keywords:
Cement
Healing
Proteins

ABSTRACT

While there has been an increasing interest in the area of biocementation for crack healing in cementitious materials, the role of biomolecules as an important constituent in biocementation has not received attention. This paper examines the interaction between proteins, with different molecular structures, and a cementitious surface that can represent a crack surface. The chemical characteristics and microstructure of the product formed on the cementitious surface were studied using Fourier transform infrared spectroscopy (FTIR), thermogravimetric analysis (TGA), X-ray diffraction (XRD), and scanning electron microscopy (SEM). The optical and X-ray micro-computed tomography (micro-CT) imaging were employed to evaluate the crack filling ability of the proteins. The crack healing property of the proteins was investigated using the three-point bend test. The samples treated with proteins demonstrated marked increase in strength recovery as well as crack filling, compared to the control sample. The molecular changes occurring in proteins when exposed to cement chemistry were shown to improve the interfacial strength between the proteins and cementitious surface. It was also found that the proteins can effectively induce hydrophobization on cementitious surface. It was shown that the surface product consisted mainly of calcium carbonate ($CaCO_3$), ettringite, and calcium-silicate-hydrate (C—S—H). The morphology of ettringite in the samples treated with proteins showed distinct differences compared to that in the control samples.

1. Introduction

Concrete is susceptible to cracking due to the mechanical loading and environmental stressors [1,2]. Formation and growth of cracks in concrete accelerate the transport of chemical and biological substances that can initiate the degradation mechanisms leading to a loss of structural integrity of concrete structures [3]. Biocementation, based on the precipitation of calcium carbonate mineral induced by biological microorganisms, has emerged as a viable method to heal cracks in concrete and restore its mechanical and durability properties [4,5]. This process involves organic biomolecules including proteins and polysaccharide, which provide skeletal support and serve as a templating platform regulating the nucleation, growth and morphology of the minerals [6–8]. Several prior studies have investigated the effect of proteins on the phase and morphology of calcium carbonate [9–11]. In addition, organic biomolecules can act as a glue binding particles together and provide adhesion and cohesion to the mineral precipitates or sediments [12–15]. The gluing effect of biomolecules in the biocementation process for the crack healing of cementitious materials has not been studied in the past and is currently unknown. In a prior study [16], researchers showed that the microbial induced calcium carbonate precipitation was able to bind loose sand particles while chemical calcium carbonate precipitation did not provide binding between the loose sand particles. In the above mentioned paper, the difference in the morphology and surface chemical characteristics of calcium carbonate precipitates were mentioned as the reason for the different binding properties of the microbial induced and chemical calcium carbonate precipitates. Although not directly pointed out by these authors, the gluing effect of the biomolecules at calcium carbonate-calcium carbonate interface as well as calcium carbonate-sand interface could be a major contributor to the binding ability of the microbial induced calcium carbonate precipitate.

The Great Wall of China built by Emperor Qin Shi Huang was constructed by large labor force who used sticky rice to bind bricks. Rice basically consists of a biogenic component called amylopectin while the bricks are mainly made up of inorganic calcium carbonate [17]. The interfacial adhesion between the organic and inorganic constituents could be a reason why this Great wall has been strong over the years [18]. Several investigations have been carried out on the development of different biomolecules, including proteins, to produce bio-based

* Corresponding author.
E-mail address: a.ghahremani@miami.edu (A. Ghahremaninezhad).

https://doi.org/10.1016/j.conbuildmat.2022.128982
Received 21 May 2022; Received in revised form 2 August 2022; Accepted 24 August 2022
Available online 6 September 2022

Table 1
Oxide composition of the type I/II ordinary Portland cement used in this study.

Oxide	CaO	SiO_2	Al_2O_3	Fe_2O_3	MgO	Na_2O	K_2O	SO_3	LOI	Total
%	64	20.6	4.8	3.5	0.9	0.3	0.1	3.4	2.4	100

adhesives [19–23].

Protein-based adhesives have attracted greater interest in the area of bio-composite production because of their rich source in providing cheap, nontoxic and renewable glues that can effectively bind inorganics together [21–23]. It has been widely applied as additives and binding agents in the area of wood and metal bonding [19–21].

Proteins are a group of biomolecules formed by a sequence of amino acids which are linked by peptide bonds. Amino acids possess side groups, which could be charged, hydrogen bond forming, or hydrophobic, permitting an array of interaction pathways between their side groups and other solid surfaces [24]. Thus, due to the heterogeneity of surface characteristics of cementitious materials, proteins have the potential to interact with cementitious surfaces in a variety of ways.

Previous studies have focused on the addition of these proteins at the casting stage of the cement/concrete. For instance, Ventola et al [25] studied the influence of proteins on the mechanical properties, carbonation resistance and porosity of lime mortars. Their outcome revealed an improved compressive strength, higher water resistance and higher carbonation resistance of the protein modified lime mortars. Brzyski et al. [26] investigated the effect of casein protein on the mechanical property of lime-metakaolin paste. It was reported that although casein protein reduced the compressive strength of the paste, the flexural strength was increased when casein protein of concentration 0.5 % was admixed. The enhanced flexural strength was attributed to the adhesion between lime particles as a result of the gluing nature of the casein protein [26]. Kamali et al. [27] studied the effect of two proteins, namely albumin and lysozyme, on the atomic structure, morphology and nanomechanical properties of C—S—H, which is the main binding phase of hydration product in cementitious materials. Prior research has documented that certain marine microorganisms, when applied to the surface of cementitious materials, have the ability to seal underlying surface cracks [28] or reduce ion permeability [29] of cementitious materials.

In spite of a large number of studies on the use of biocementation for crack healing in cementitious materials [2,4,5,30], there is a lack of knowledge in the specific area of the interaction between proteins and aged cementitious surface that can represent a crack surface. Therefore, this paper aims to address this knowledge gap and investigate how proteins affect the microstructure and chemical characteristics of the products formed on the surface of cementitious materials, the interfacial strength between proteins and cementitious surface, and strength recovery and crack filling of cracked cementitious materials. In this study, the effect of five proteins possessing different molecular structures is examined. The presence of various functional groups in their molecular structure and charge variations equip proteins with various interaction pathways with surface products. Calcium ions diffuse through proteins and react with carboxylate groups to form networked complexes [31]. These interactions enable the proteins to self-assemble to form gels which can serve as a glue. The effect of cement chemistry on the physicochemical properties, including surface charge, hydrodynamic size, and surface tension of the proteins was evaluated. FTIR, TGA, XRD, and SEM were used for the microstructure characterization of the surface product treated with proteins; optical and micro-CT imaging were employed to evaluate the crack filling of the samples treated with the proteins. The contact angle and water absorption of the samples treated with proteins were also evaluated.

2. Experiments

2.1. Materials

2.1.1. Proteins

Five different proteins, namely whey protein, albumin, non-fat milk powder (NFMP), sodium immunoglobulin (SBI), and collagen peptide (CP), with different functionalities and molecular structures were purchased from the commercial vendors. These proteins were used based on their commercial availability and utilization in other studies. With the exception of CP, which has been reported to be fibrous, whey protein, albumin, NFMP, and SBI are classified as globular proteins in their native state [32–34]. SBI is made up of about 90 % protein and is obtained by separating edible grade bovine plasma [35]. NFMP is prepared from non-fat milk and possesses 34–36 % protein on dry mass [36]. Whey protein concentrate is a by-product of the cheese making process [32]. The albumin used is made up of ovalbumin, which comprises about 54–58 % by weight of the egg white protein [37]. Collagen on the other hand is a structural protein whose amino acid make-up is uniquely distinct from other proteins. The high content of hydroxyproline and proline restricts the protein from forming a globular shape. Nonetheless, there is a good interaction among the polar chains of the collagen [24].

2.1.2. Cement paste

A type I/II ordinary Portland cement (OPC) was used in the preparation of cementitious surface and cracked cement paste prisms. The chemical composition of the type I/II OPC is shown in Table 1.

2.1.3. Sample preparation for chemical and microstructural analysis

Samples for the microstructure and chemical characterization (FTIR, TGA, XRD, SEM) of the surface product were prepared by cutting cement paste prepared with a water to cement ratio (w/c) of 0.4 into pieces of dimensions 25 mm × 10 mm × 25 mm. Before cutting, these samples had been cured for 3 days. The surface of the cut samples was polished with SiC sand papers with grit numbers of 320, 500, and 1200, and finely polished with a 1 μm diamond abrasive paste. After polishing, the samples were dried in a vacuum oven for 6 h and then, submerged in a synthetic pore solution (SPS) containing the proteins with a concentration of 2 % by mass. Two control samples were submerged in de-ionized water only (DW) or SPS only without proteins. Synthetic pore solution was utilized in this study to evaluate the effect of high pH and ionic composition on protein response. The SPS used was prepared to contain 0.02 M $Ca(OH)_2$, 0.037 M Na_2SO_4, 0.1062 M KOH, and 0.037 M K_2SO_4 following the procedure described in [38]. Samples were removed after 1 h of treatment time and then exposed to laboratory condition with 0.043 % CO_2 for 3 and 28 days, respectively, until testing. Prior to the chemical and microstructural characterization, the samples were dried in a vacuum oven at 50 °C for 24 h.

2.2. Methods

2.2.1. Zeta potential and hydrodynamic size

Investigation was carried out to evaluate the net surface charge and the hydrodynamic size of the proteins using dynamic light scattering in a Zetasizer Nano ZS instrument (Malvern Instruments ltd., Malvern, U.K.) conditioned at 25 °C. The measurement parameters, namely refractive index (RI) and absorption coefficient, for the proteins were set at 1.45 and 0.001, respectively. For zeta potential and hydrodynamic size measurements, 0.15 % concentration of protein by mass of DW at the native state and at pH level of 13 was prepared and equilibrated prior to

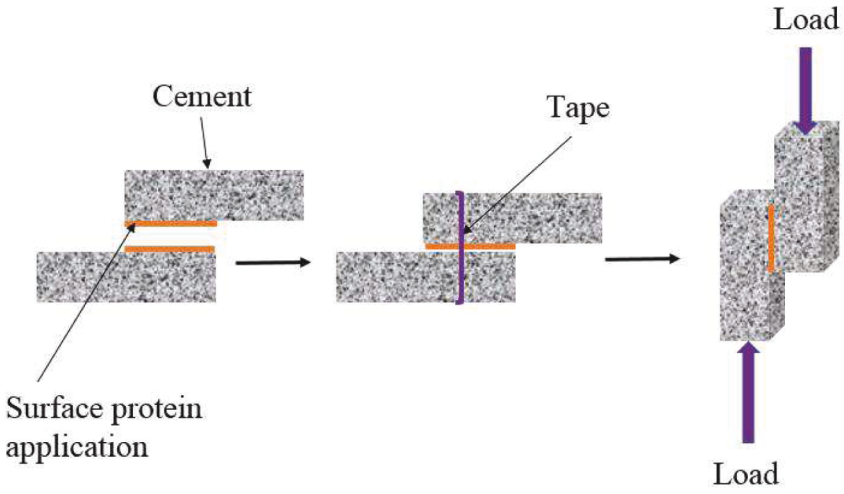

Fig. 1. Schematic diagram of the interfacial strength test.

testing. After 10 min of equilibration, the protein solution was filled in a disposable folded capillary cell (DTS1070) and loaded into the instrument. After loading into the instrument, the samples were equilibrated for 120 s before testing. Each sample was tested three times and in between each test, data was collected after 100 or 110 runs.

2.2.2. Surface tension

Surface tension of the protein solutions was measured to provide information about the surface hydrophobicity of the proteins in both DW and SPS. Solutions with protein concentrations of 0.25 %, 0.5 % and 1 % by mass of DW and SPS were prepared and allowed to equilibrate for 10 min. Surface tension values were measured with the KRÜSS Digital Tensiometer K10S using the ring method. The diameter and thickness of the ring was 9.36 mm and 0.37 mm, respectively. Before each run, the ring was thoroughly heated by a wick flame and cleaned with acetone to remove organic contaminants. Three replicates were tested for each sample and the average reported.

2.2.3. FTIR

FTIR was employed to characterize the products formed on the cementitious surface treated in DW only, SPS only, and SPS with proteins. The surface product of the treated cement paste samples was scraped, ground, and passed through sieve # 60. Approximately, 30 mg of the fine surface product was utilized in the test. FTIR measurements were performed using a Perkin Elmer Paragon 1000 FTIR with an ATR accessory in a transmission mode. The scan resolution was 4 cm^{-1} and spectra were recorded between 600 cm^{-1} and 4000 cm^{-1}. Each sample was taken through 4 scans and an average of two samples from the 4 rounds of scans was reported for analysis.

2.2.4. TGA

The sample preparation for TGA was similar to that for FTIR, as described previously. About 30 mg of the fine product was loaded into a Netzsch TGA and scanned at a heating rate of 20 ºC/min between 30 ºC and 900 ºC under a flow of Argon gas. Two replicates of each samples were used and the average reported.

2.2.5. XRD

The mineralogical composition of the product formed on the cementitious surface treated in DW only, SPS only, and SPS with proteins was evaluated using a Rikagu X-ray Diffractometer (Model D/Max-3C, Rikagu, Japan). The scanning was performed using Cu Kα radiation at 40 kV and 40 mA, with a scan interval of $2\theta = 10^{\circ}$ to 80°, and a step size of 0.0194°/s. For the XRD analysis, small blocks with dimensions of 10 mm × 10 mm × 10 mm were cut from the 3-day and 28-day cured cement paste samples and vacuum dried for 24 h. The samples were then placed inside a sample holder and inserted into the device, and the surface of the sample was scanned.

2.2.6. SEM

The SEM images of the surface of the cement paste cured for 3 days and treated in DW only, SPS only, and SPS with proteins were obtained using a Zeiss Gemini Ultra Plus FESEM in the secondary electron mode. Prior to taking the SEM images, the cementitious surface was sputter coated with a thin layer of gold to prevent charging in imaging at higher kV and magnification. The accelerating voltage was 10 kV at a working distance (WD) of 10 mm. Images were taken at the magnifications of 20 kX and 200 kX.

2.2.7. Contact angle measurement

The contact angle between DW and cementitious surface was measured by a simple apparatus comprising a dropper and a higher resolution camera. Cement paste samples of dimensions 5 mm in height and 12.5 mm in diameter cured for 3 days were utilized in this experiment. Before treating the cement paste in the various protein solutions, the samples were polished using SiC sand papers with grit numbers of 320, 500, and 1200, and finely polished with a diamond abrasive paste of particle size 1 μm. The polished samples were dried at 50 °C in a vacuum oven for 24 h. The samples were then submerged in DW only, SPS only, and SPS with proteins for 1 h and then exposed to ambient condition for 7 days and 28 days, respectively. Approximately 5 μL of DW droplet was cast on the treated cementitious surface using a dropper. Images of the shape of the stable DW droplets on the cementitious surface were taken using a high-resolution camera. The angle between the surface of the droplet and the surface of the cementitious surface was measured using the image J software. Approximately 20 different contact angles were measured for each sample and the average reported.

2.2.8. Water absorption

The water absorption of the control and protein treated cement paste was determined following the ASTM C1585-13. Cement paste samples cured for 3 days and 28 days were cut into pieces with dimensions of 25 mm × 20 mm × 20 mm. One side of the samples was polished using SiC sandpapers with grit numbers of 320, 500, and 1200, and followed by polishing with a 1 μm diamond abrasive paste. The polished samples were vacuum-dried at 50 °C for 24 h and then treated in SPS only and SPS with proteins for 1 h. SPS was used to mimic the chemistry of cement pore solution. After one hour of treatment, the samples were

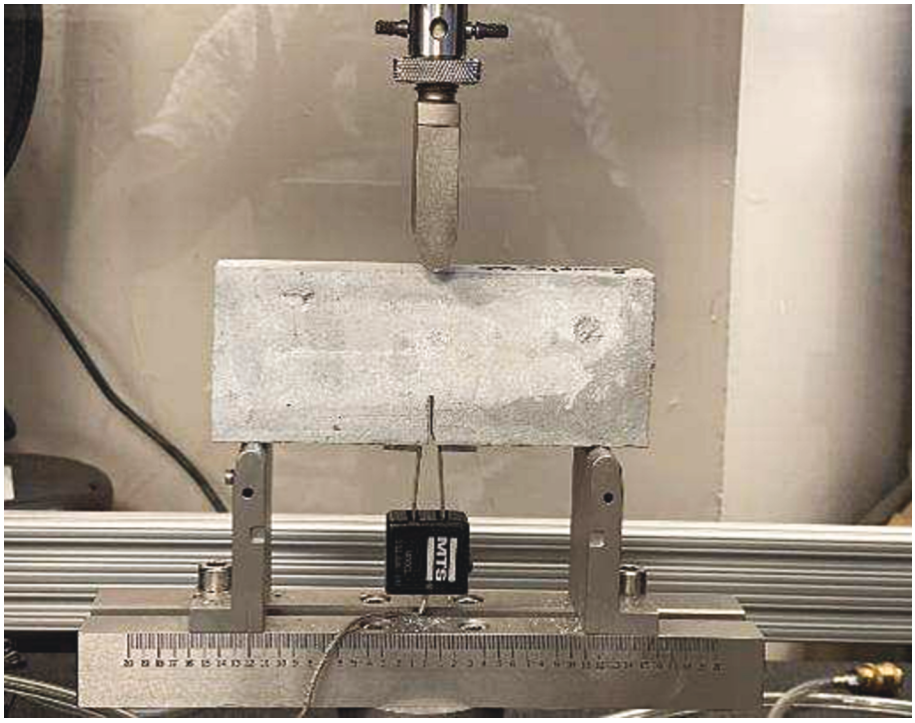

Fig. 2. Setup for three-point bend test of the cement paste prisms.

taken from the various solutions and exposed to the ambient conditions for 3 days. The samples were then dried in a vacuum oven at 50 °C for 24 h. After oven drying, all sides of the samples except the polished side were sealed with an aluminum tape. This was done to ensure a unidirectional water transport through the unsealed side of the samples. The unsealed side of each sample was placed on a mesh mounted in a graduated container containing DW. The submerged depth of the samples was 2 mm. Sample mass was measured after 10, 20, 40, 90, 150, 240 and 360 min of partial immersion. The samples were wiped of water before each measurement. This process was repeated for the 28-day cured samples. The water absorption was determined using equation (1).

$$I = \frac{(m_i - m_0)}{6.25}$$

where m_0 and m_i is the mass of the sample at time zero and different times during water uptake, respectively.

2.2.9. Interfacial strength test

The interfacial strength between the cementitious surface and proteins was evaluated using the lap shear test. Cement paste specimens used for the lap shear test were prepared by mixing cement with DW using a water to cement ratio (w/c) of 0.4. The cement paste was cast in a prismatic metallic molds with dimensions of 50 mm × 25 mm × 300 mm, covered with plastic sheet and cured for 24 h. After 24 h, the prisms were demolded, wrapped in plastic bag, and left to further cure in a humidity chamber until 3 days and 28 days. Then, cement paste pieces with the dimensions of 50 mm × 25 mm × 25 mm were cut from the prisms using a diamond saw and surface polished using SiC paper with grit sizes of 320 and 500. In order to examine the effect of protein concentration on interfacial strength, protein solutions were prepared with DW with different concentrations of 0.12 g/mL, 0.16 g/mL, and 0.24 g/mL. Approximately 500 μL of the protein solution was spread using a pipette over an area with dimensions of 30 mm × 30 mm between two cement paste pieces in a single lap mode as shown in Fig. 1. The samples were pressed firmly together at the interface region with a rubber band and left to cure in the oven at 38 °C for 23 h followed by 15 min cooling.

In addition, in order to investigate the effect of the chemistry of the solution on the interfacial strength, protein solutions were prepared with DW, SPS, and alkaline solution with a pH of 13.6. The alkaline solution had a similar pH to SPS but did not contain the ions that were present in SPS; thus, allowing to study the effect of ions in solution. The cement paste pieces used with these protein solutions were immersed in acetone for 24 h and then, dried in a vacuum oven for 6 h before the protein solutions were applied to them. The interfacial strength test was performed using an Instron testing machine at a displacement rate of 0.05 mm/sec. Five replicates of each samples were tested and the interfacial shear strength σ_s was calculated by equation (2) [39] as follows:

$$\sigma_s = \frac{N_{max}}{A_b} \quad (2)$$

where N_{max} is the maximum shear load (N) attained before failure and A_b is the surface area of the interface region in mm^2.

2.2.10. Crack healing evaluation

Mortar prisms with the dimensions of 150 mm × 55 mm × 25 mm, with a water/cement of 0.5, sand/cement of 2 were cast and cured for 28 days. The sand used consisted of fine quartz sand with a size in the range of 0.15 mm-0.5 mm. A notch with a width and length of 2 mm and 14 mm, respectively, was introduced in the middle of the top surface of the prisms using a diamond saw. The prisms were loaded in the three-point bend mode setup to grow a single crack with a mouth opening displacement (CMOD) of approximately 100 μm. The CMOD was monitored using an MTS extensometer attached to two small metal plates attached close to the notched area (see Fig. 2). The two metal plates served as contact points for the pins of the extensometer as the notch width was too small to accommodate the pins of the extensometer. Loading was performed using an Instron testing machine at a displacement rate of 0.0001 mm/sec. The target CMOD corresponded to approximately 90 % of the peak load of the prisms. After unloading, the images of the single cracks were taken using the KEYENCE VHX 5000 microscope at a magnification of 200x. The cracked prisms were

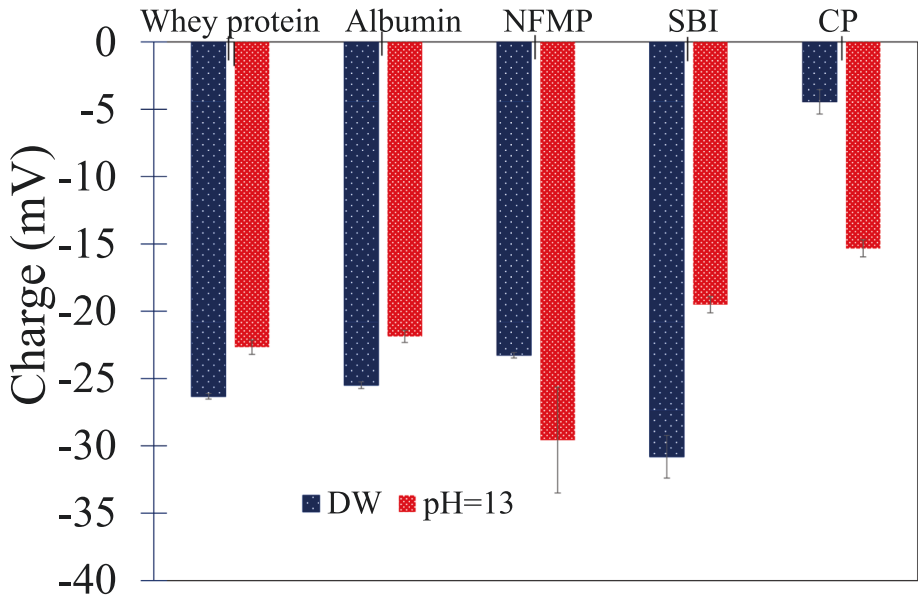

Fig. 3. Zeta potential measurement of proteins in DW (native state) and pH level 13.

subjected to 14 days of dry/wet cycles at room temperature of 25 °C. In the wet cycle, the prisms were submerged in DW and DW containing proteins at a concentration of 3 % by mass of DW. The healing procedure consisted of partially submerging the prisms in the respective solutions for 3 h (wet cycle) and exposing them to the ambient conditions for 21 h (dry cycle). On the 14th day, the prisms were left to dry under ambient condition for additional 24 h and then their surfaces were imaged for crack filling examination. Images of the cracked prisms after the healing process were compared to the images of cracked samples before healing. Then, the prisms were loaded in a three-point bend mode until complete failure. Five replicates subjected to each protein solution were tested and the average reported. The strength recovery ratio of each healed prism was determined using equation (3):

$$Strength\ \ recovery\ \ (\%) = \frac{P_{max,reloading} - P_{unloading}}{P_{max,uncracked} - P_{unloading}} \quad (3)$$

where

$P_{max,reloading}$ is the maximum load obtained after healing,
$P_{max,uncracked}$ is the maximum load of the uncracked sample,
$P_{unloading}$ is the residual load obtained before unloading.

2.2.11. Micro-CT analysis

Micro-CT was employed to investigate the internal crack filling in the samples. Since the optical imaging only allows the imaging of the cracks on the surface of the samples, micro-CT can provide useful information regarding the internal condition of the cracks. The sample preparation followed that used in the three-point bend samples to introduce a single crack in the samples. The samples were then subjected to wet/dry cycle in different solutions as described in the three-point bend test. Only the samples treated in DW, NFMP, and SBI were used in the micro-CT analysis. Samples before and after healing were scanned using the Bruker Skyscan 1273 (Bruker, Kontich, Belgium) at a scanned resolution of 27 μm/pixel with a 2 mm Copper filter. The exposure time, average frame, rotational step, voltage and current were 4350 ms, 8, 0.6°, 130 kV and 115 μA, respectively. The samples were held firmly in a polyethylene filled with a Styrofoam. The samples were placed between an X-ray source and an X-ray detector and scanned for a period of approximately 4 h during which about 345 projections over 180° were taken. Before scanning the healed samples, they were oven-dried at 44 °C for 24 h to remove moisture. A 3-D analysis of the reconstructed images was quantitatively performed using the CTAnalyzer software (1.20.8). Segmentation of the samples into solid matrix and void was done using the grey scale intensity thresholds with the grey scale range of 0–70 representing voids. To visualize the cracks in 3-D, the CT-volume was utilized to reconstruct the 3-D models produced by the CTAnalyzer software.

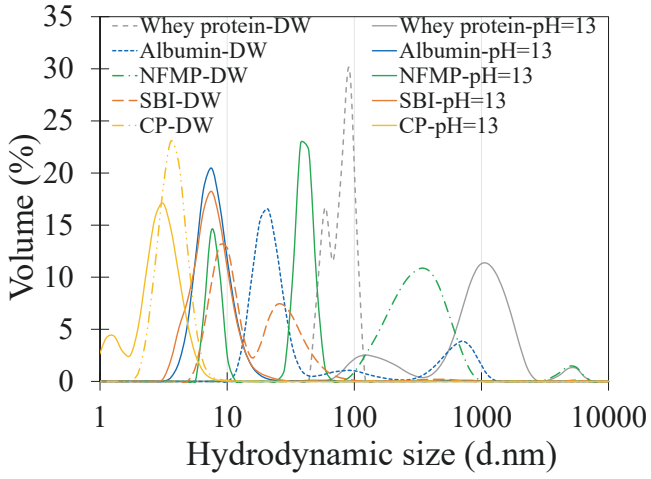

Fig. 4. Hydrodynamic size measurement of proteins in DW (native state) and at pH level of 13.

2.3. Results and discussions

2.3.1. Zeta potential and hydrodynamic size

Fig. 3 illustrates the zeta potential of the proteins in DW (native state) and at pH level of 13. It can be seen that whey protein, albumin and SBI showed reduced anionic charge as the pH level was increased to 13. The anionic charge of whey protein, albumin and SBI decreased from −26.3 mV to –22.7 mV, −25.5 mV to −21.9 mV and −30.8 mV to −19.5 mV, respectively. This behavior was opposite to the charge behavior of CP and NFMP, which showed an increased anionic charge from −4.4 mV to −15 mV and –23.3 mV to −29.6 mV, respectively. The surface charge of proteins typically increases due to the amino acid deprotonation as the pH increases [40,41]. Under severe pH condition, the proteins undergo some conformational and molecular changes [42]. As the proteins

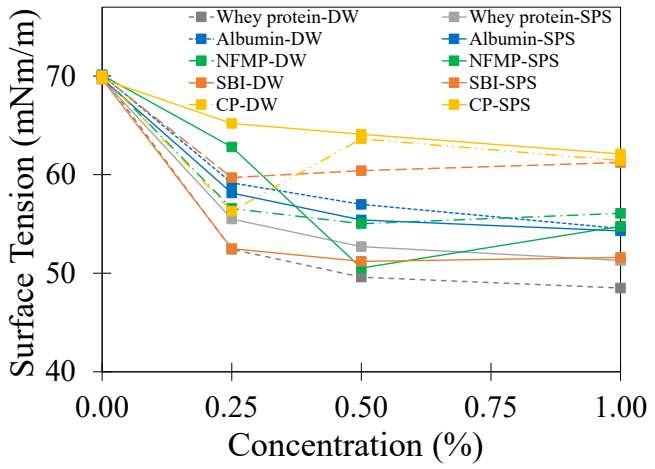

Fig. 5. Surface tension measurement of protein solutions in DW (native state) and SPS.

undergo these changes, the various molecular bonds including disulfide bonds, hydrogen bonds, hydrophobic bonds and van der Waals bonds break, and this leads to the breakup of the molecular chain of the proteins into smaller units [41,43]. It can be suggested that the observed reduction in the anionic charge of albumin, whey protein and SBI at the pH level of 13 could be attributed to the association of the dissociated protein subunits at the very high pH level of 13. During the association, charged amino acids may be enclosed inside the interior of the protein and may not contribute to the ultimate surface charge of the proteins [40]. As is the case, it is noticed that the charge of NFMP remained consistently high even at pH level of 13. NFMP is composed of a significant amount of casein [36]. At the pH level of 13, the degree of deprotonation of amino acid residues in the casein is further increased and that results in an increased charge of the NFMP. This result is consistent with the observations made by Bian [40] who reported an increased charge of casein when the solution pH of the protein was increased from 12 to 13.

The hydrodynamic size of the proteins in DW and at pH level of 13 is shown in Fig. 4. It is seen that the hydrodynamic size of albumin, NFMP and SBI was higher in DW compared to their sizes at pH level 13. It is however noticed that whey protein showed an increased hydrodynamic size at pH level 13 compared to its size in DW. The observed decrease in hydrodynamic sizes of albumin, NFMP and SBI can be attributed to the dissociation of the proteins into subunits at the pH level of 13 [44]. In the case of whey protein, it could be suggested that the observed increase in size at pH level 13 may be attributed to the association of the dissociated whey protein subunits as conformational changes could be partially reversible [40,41]. In addition, since these proteins were purchased and utilized as received, some impurities may be present, and these impurities may be favorable towards the assembly of the subunits of whey proteins at higher pH level compared to the native state [41]. It is seen that the hydrodynamic size of CP did not vary significantly with pH. This observation could be due to the fact the intermolecular forces in the case of CP were weak and could not promote aggregation or repulsion.

2.3.2. Surface tension

The surface tension of the protein solutions was measured to study the hydrophobic property of the proteins in DW and SPS. A direct correlation between surface tension and surface hydrophobicity was made in previous studies [41,45,46] indicating a decrease in the surface tension of protein solutions with increased surface hydrophobicity of proteins. Zecca [47] also reported in a study that surface tension is a reliable measure to evaluate the surface hydrophobicity of proteins. Different parameters including temperature, concentration, pH and ionic

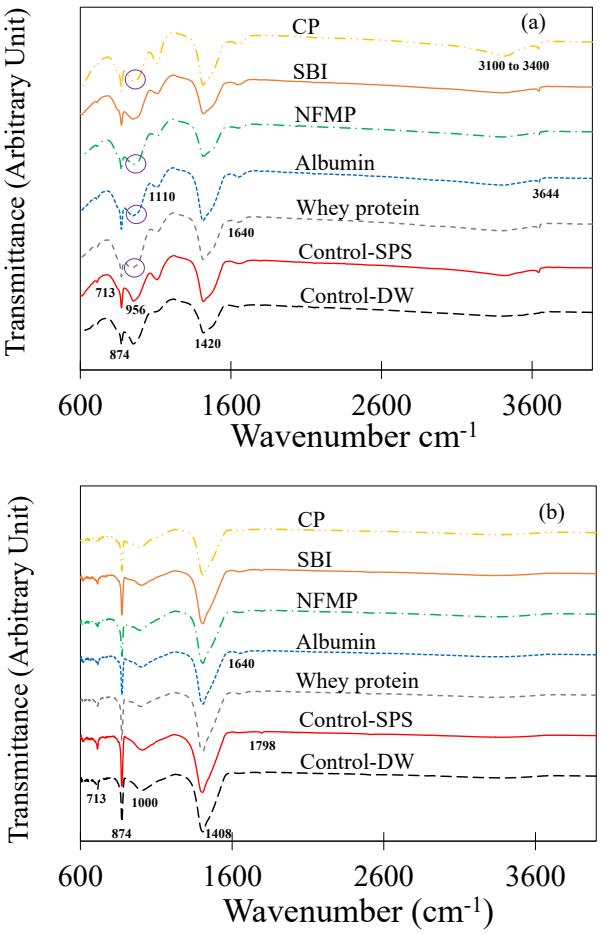

Fig. 6. FTIR spectra of (a) 3-day and (b) 28-day treated samples.

composition influence surface hydrophobicity of proteins [48]. Modification of the molecular structure of proteins due to denaturation, leads to changes in the distribution of hydrophobic groups in the proteins surface [49]. It is seen from Fig. 5 that the proteins exhibited different surface tension behaviors in DW and SPS. It is also observed that the effect of SPS on the surface tension appeared to be different among the proteins studied here. It is seen that SBI demonstrated a noticeable reduction in surface tension in SPS compared to in DW; NFMP showed a slightly lower surface tension in higher concentrations in SPS than in DW. Albumin did not show significant difference in surface tension in DW or SPS. On the other hand, whey protein showed a lower surface tension in DW compared to in SPS. CP exhibited a lower surface tension in DW compared to in SPS in low concentrations but the difference diminished with an increase in concentration.

SPS has a pH of 13.6 and contains several ions including K^+, Na^+, and Ca^{2+}. The observed surface tension behaviors of the proteins in SPS compared to DW is due to the elevated pH level of the SPS as well as the interactions between ions and proteins. In their native state in DW, proteins fold into a globular morphology due to the intermolecular forces [50,51]. In this state of protein morphology, the hydrophobic groups reside in the interior of the protein molecules while the hydrophilic groups are situated on the outside of the protein molecule. When the pH is increased to a level as high as the pH of SPS, proteins undergo conformational changes and begin to unfold to expose the hydrophobic groups [52–54]. The exposed hydrophobic groups tend to adsorb to the air–water interface and reduce the surface tension of the protein solutions [41,44]. Increased hydrophobicity of proteins at high pH has been observed in the previous studies [55–57]. On the other hand, protein aggregation and other potential molecular changes due to increased pH

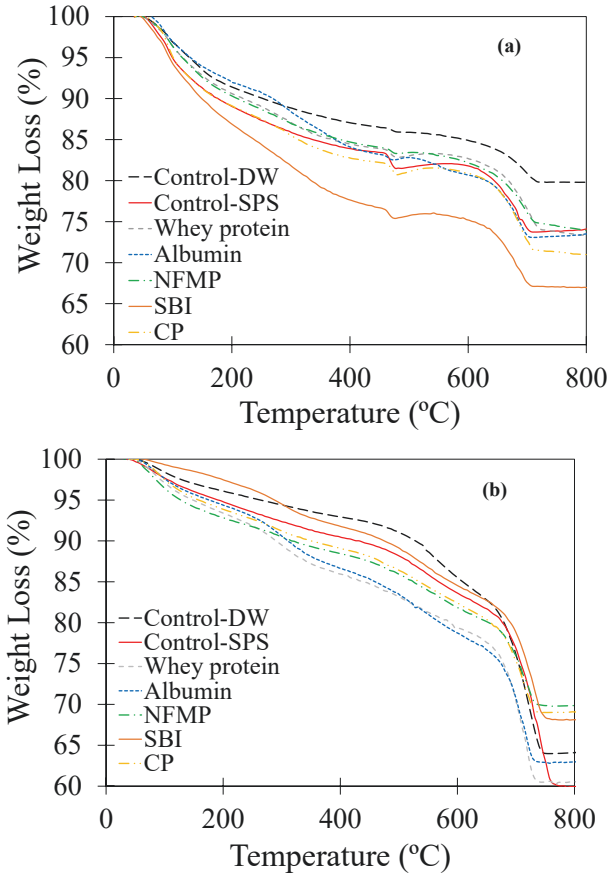

Fig. 7. TGA and DTG curves of (a) 3-day and (b) 28-day treated samples.

or interaction with ions could reduce the exposure of hydrophobic groups in proteins resulting in increased surface tension of the protein solutions. Thus, the above mentioned processes, which have opposing influences, are responsible for the different surface tension behaviors of the proteins in DW and in SPS. In the native state in DW, it is observed that whey protein showed a lower surface tension compared to the value obtained in SPS. This could be due to aggregation in whey protein as demonstrated by its increased hydrodynamic size at high pH in Fig. 4. The observed high value of surface tension of CP in both DW and SPS may be attributed to a lower composition of hydrophobic amino acid groups in the molecular structure of CP.

2.3.3. FTIR

FTIR spectra were collected to examine the chemical characteristics of the product formed on the surface of the cement paste treated with and without proteins. Fig. 6a and b illustrate the FTIR spectra of the product after exposing the treated samples to ambient conditions for 3 days and 28 days, respectively. The small peak located at 713 cm^{-1} and the sharp peak at 874 cm^{-1} in Fig. 6a correspond to calcite [58–60]. In Fig. 6b, the peaks located at 713 cm^{-1} and 874 cm^{-1} appeared sharper and much more intense indicating an increased carbonation reaction for the 28-day old-treated samples. It is however noticed that protein treated samples in Fig. 6b showed lower intensity for this peak, compared to the control sample possibly due to the reduced surface area for carbonation reaction as a result of the adsorption of the proteins onto the cementitious surface.

The peak located at 956 cm^{-1} is assigned to the stretching vibration of Si-O-Si, which can be attributed to C—S—H in the samples [61]. It is seen that, the Si-O-Si vibration peak in the sample treated with proteins appeared smaller than that in the control sample (Fig. 6a). This could possibly be attributed to the delayed hydration of unhydrated cement

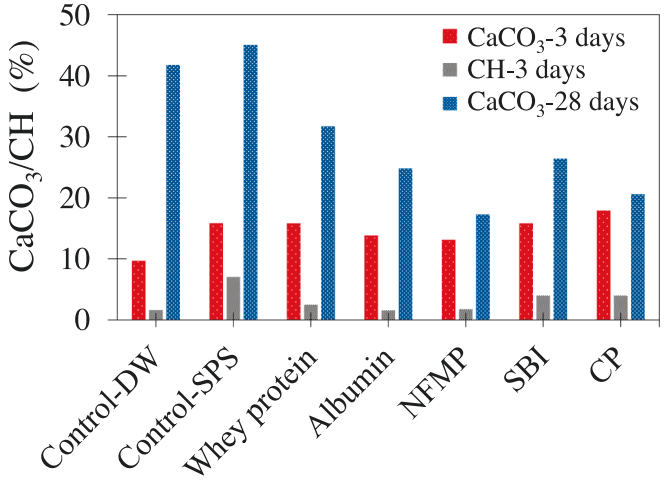

Fig. 8. TGA quantification of CH and $CaCO_3$ contents.

particles on the surface due to the adsorption of proteins. It is instructive to note that the Si-O-Si peak in the surface product corresponding to 3-day treatment shifted from 956 cm^{-1} to 1000 cm^{-1} in the case of 28-day treatment. This could be due to the decalcification of C—S—H and formation of polymerized silicate gel in the 28-day treated samples [62,63]. The characteristic peak at 1110 cm^{-1} of the control (SPS) and protein treated samples can be assigned to the S—O stretching vibration of SO_4^{-2} [41,59,64,65]. The S—O peak was less pronounced in the control (DW) samples, indicating the presence of smaller amount of ettringite. Interestingly, the S—O peak disappeared after the 28-day treatment period. This peak is stabilized by increased pH of the cementitious environment however, due to carbonation of CH and other alkalis, there is a drop in pH of the cementitious environment leading to the dissolution and carbonation of this phase. With prolonged exposure to atmospheric CO_2, the ettringite converts to $CaCO_3$, gypsum and water [66].The peaks ranging between 1408 cm^{-1} and 1420 cm^{-1} for the samples are attributed to the v_3 CO_3^{-2} bands [41,61,64] and they appeared more intense in the 28-day treated samples due to prolonged carbonation. The peaks located at 1640 cm^{-1} and between 3100 cm^{-1} to 3400 cm^{-1} is assigned to the bending vibration of OH^- [41,64,67]. The OH^- and amide I bands have overlapping peaks at 1640 cm^{-1} [41,68–70], but considering the corresponding OH^- peak between 3100 cm^{-1} to 3400 cm^{-1}, these peaks may be related to the presence of bound water. The peak at 3644 cm^{-1} for the 3-day treated samples corresponds to the O—H bond in CH [41,58,71]. The obvious disappearance of the CH peak for the 28-day treated samples confirms the transformation of CH to $CaCO_3$.

2.3.4. TGA

Fig. 7a and b illustrate the TGA curves of the samples treated for 3 days and 28 days, respectively. The mass loss at 70 °C and 180 °C correspond to ettringite (AFt) and monosulfate (AFm), respectively [41,72]. The loss of chemically bound water from C—S—H occurred around 110 °C and 200 °C [41,72]. Fig. 7a shows a noticeable weight loss in most of the samples as the temperature increased from about 420 °C to 480 °C. This weight loss is attributed to the decomposition of CH [41,72]. The absence of this weight loss in Fig. 7b is attributed to the carbonation of CH due to prolonged carbonation reaction. This corroborates the findings of the FTIR results, discussed previously. Furthermore, a weight loss occurred within the temperature range of 580 °C and 720 °C. The weight loss is attributed to the decomposition of $CaCO_3$ [41,72]. The weight loss appeared more noticeable in the 28-day treated samples due to the presence of more carbonated phases.

The quantification of CH and $CaCO_3$ content is shown in Fig. 8. It is observed that SPS influenced the amount of $CaCO_3$ and CH formed possibly due to high pH (13.6) and provision of Ca^{2+} from SPS into the

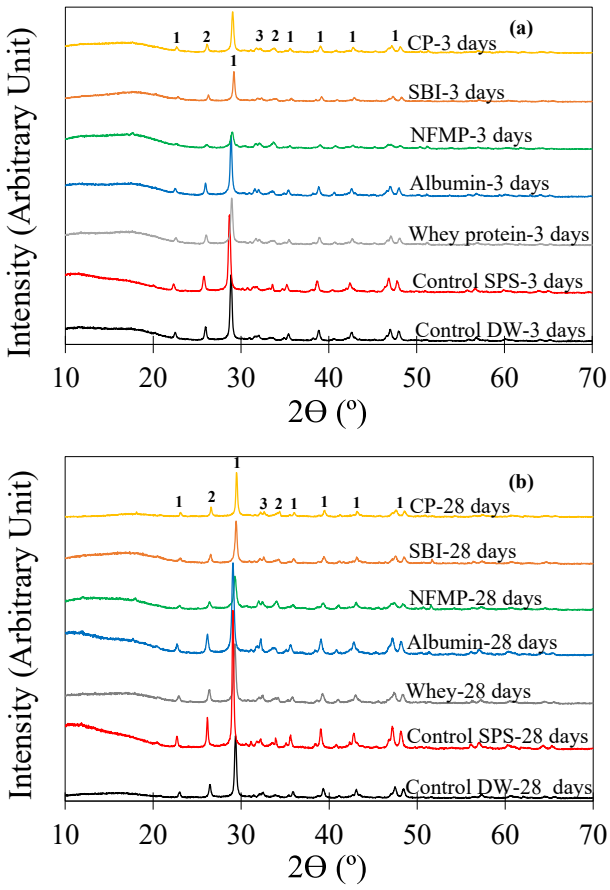

Fig. 9. XRD spectra of (a) 3-day and (b) 28-day treated samples. 1 = Calcite, 2 = Vaterite, and 3 = Belite.

surface product. From the results, it is observed that albumin, NFMP and SBI showed lower $CaCO_3$ formation in both treatment durations. At high pH, the carboxylate groups of the proteins are highly negatively charged and can electrostatically bind with Ca^{2+} to form complexes [41,73]. In addition, the negatively charged carboxylate groups can interact with negatively charged silicate phases of the hydrating cement particle through the bridging effect of Ca^{2+} [41]. The binding between negatively charged carboxylate groups of the proteins and Ca^{2+} reduces the availability of free Ca^{2+} in the mixture to participate in the carbonation process and hence a reduction in the $CaCO_3$. This result is in agreement with prior investigations [70]. Khan et al. [70] investigated the influence of biomolecules (amino acids) on the carbonation of wollastonite and observed a lower degree of carbonation in samples modified with amino acids. They attributed the reduction to the binding of the carboxyl group of the amino acid with the Ca^{2+} present in wollastonite.

2.3.5. XRD

The XRD spectra of the surface products on the samples treated for 3 days and 28 days are illustrated in Fig. 9a and b, respectively. Belite showed a weak peak at 2θ of 32.5° among all the samples [74]. Peaks associated with carbonation products can be observed in the spectra. Among the carbonated peaks detected, two polymorphs associated with $CaCO_3$ namely, vaterite and calcite, were identified. The presence of calcite is associated with the strongest peak located at 2θ of 29.4° along with many weak peaks [74,75]. On the other hand, vaterite showed a strong peak at 2θ of 27.0° as well as a peak at 2θ of 32.8° [74]. The presence of carbonate peaks as the predominant phase in the analysis is attributed to the natural carbonation of the cement paste surface region [76]. In support of this, there is a noticeable disappearance or weak peaks associated with CH and C—S—H. This behavior may be attributed to the transformation of CH and decalcification of C—S—H into $CaCO_3$ [74,76]. This is consistent with the findings of the TGA and FTIR results particularly the results for the 28-day treated samples. Generally, it is seen that the 28-day treated sample showed higher peak intensities corresponding to $CaCO_3$ compared to the 3-day treated cement paste. The polymorphs of $CaCO_3$ as indicated before consisted of vaterite and calcite with calcite being the predominant polymorph. The appearance of these peaks is consistent with the findings of [74]. It has been reported that calcite is precipitated as a result of the carbonation of C—S—H and CH while vaterite is formed as a result of the carbonation of C—S—H only [77]. Ettringite, CH, and C—S—H, which were identified in the FTIR and TGA analyses of the 3-day treated samples appeared weaker in the XRD analysis. Interestingly, samples treated with proteins showed lower $CaCO_3$ intensities compared to the control samples in both curing durations. This is in accordance with the findings of the FTIR and TGA results. The adsorption of the proteins onto the cement paste surface could reduce the surface area available for reaction, which resulted in reduced carbonation. An examination of the XRD spectra indicated that the presence of proteins did not result in production of a new phase in the surface products and all spectra showed similar features.

2.3.6. SEM

The SEM micrographs were used to investigate the effect of proteins on the morphology of the surface products of the 3-day treated cementitious surface. As shown in Fig. 10a and b, the SEM image of the control sample treated with DW only showed the formation of phases including CH, ettringite, and C—S—H. CH appeared as hexagonal shaped platelets, which has been documented as the characteristic morphology of CH in the literature [71,78]. Accurate identification of $CaCO_3$ from the images of the samples obtained from SEM was found to be difficult as $CaCO_3$ could be mixed with other phases. Ettringite appeared as a rod-like feature in the microstructure of all samples treated with and without proteins. The presence of ettringite seems to be more pronounced in the control sample treated with SPS only compared to the control sample treated with DW. This observation is in line with the weak sulfate peak associated with the FTIR of the DW treated sample as discussed in Fig. 6a. At the initial stage of hydration, C—S—H is formed with a needle-like or fiber morphology [78]. This structure gradually transforms into poor crystalline closely packed isometric grains as can be seen in the image. The microstructure of Control-SPS and some of the protein treated cement pastes showed an increased formation of ettringite compared to Control-DW. The high alkalinity of SPS and also the presence of some of the proteins seemed to favor the formation of ettringite in these samples at 3 days. An increase in ettringite formation due to the presence of proteins was also documented in a previous work by Baffoe and Ghahremaninezhad [41]. Liu et al. [79] observed a higher ettringite content in paste with a polymeric admixture compared to the paste without a polymeric admixture. A close examination of the SEM images shows differences in the morphology of ettringite in the samples treated with proteins compared to the sample treated without proteins. The surface of ettringite in the samples treated with albumin (Fig. 10g and h) and SBI (Fig. 10*k* and l) demonstrated a higher roughness compared to other samples. This could be due to protein adsorption onto ettringite in these samples. Modification of ettringite crystal due to polymeric adsorption has been observed in prior studies [79–81]. It can be seen from Figures (Fig. 10e–l) that the ettringite formed in the protein treated samples, specifically albumin, NFMP, whey protein and SBI were small rod-shaped and with a length smaller than that in the samples treated without proteins (see Fig. 10a - d). Modification of ettringite was weak in the case of CP treated samples (Fig. 10m and n) possibly due to weaker adsorption of CP onto ettringite.

2.3.7. Contact angle

Fig. 11 shows the images of DW droplets in contact with cement paste surface treated with various protein solutions. The contact angle measurements of the samples treated for 7 days and 28 days,

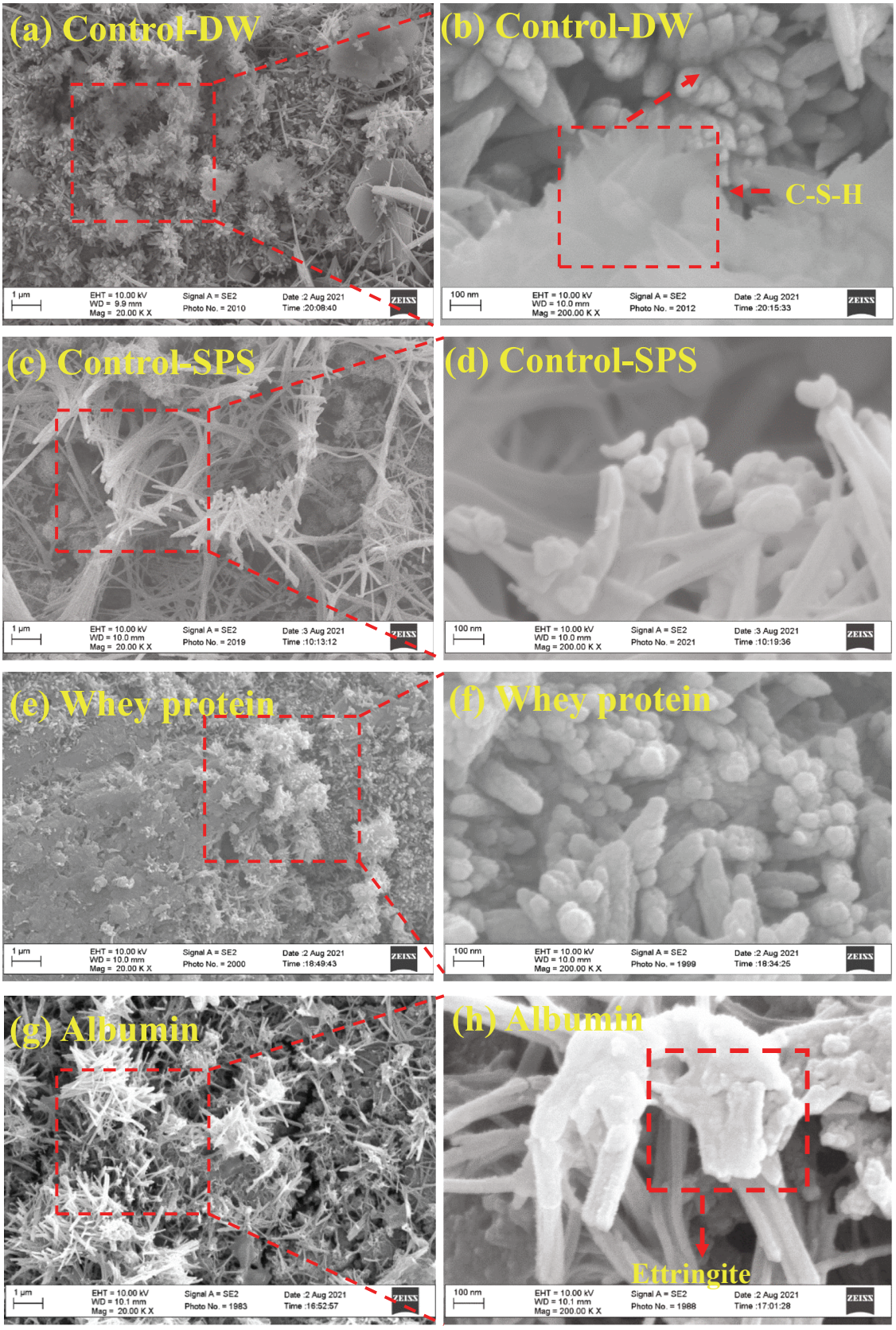

Fig. 10. SEM of cementitious surface treated with different proteins cured for 3-day.

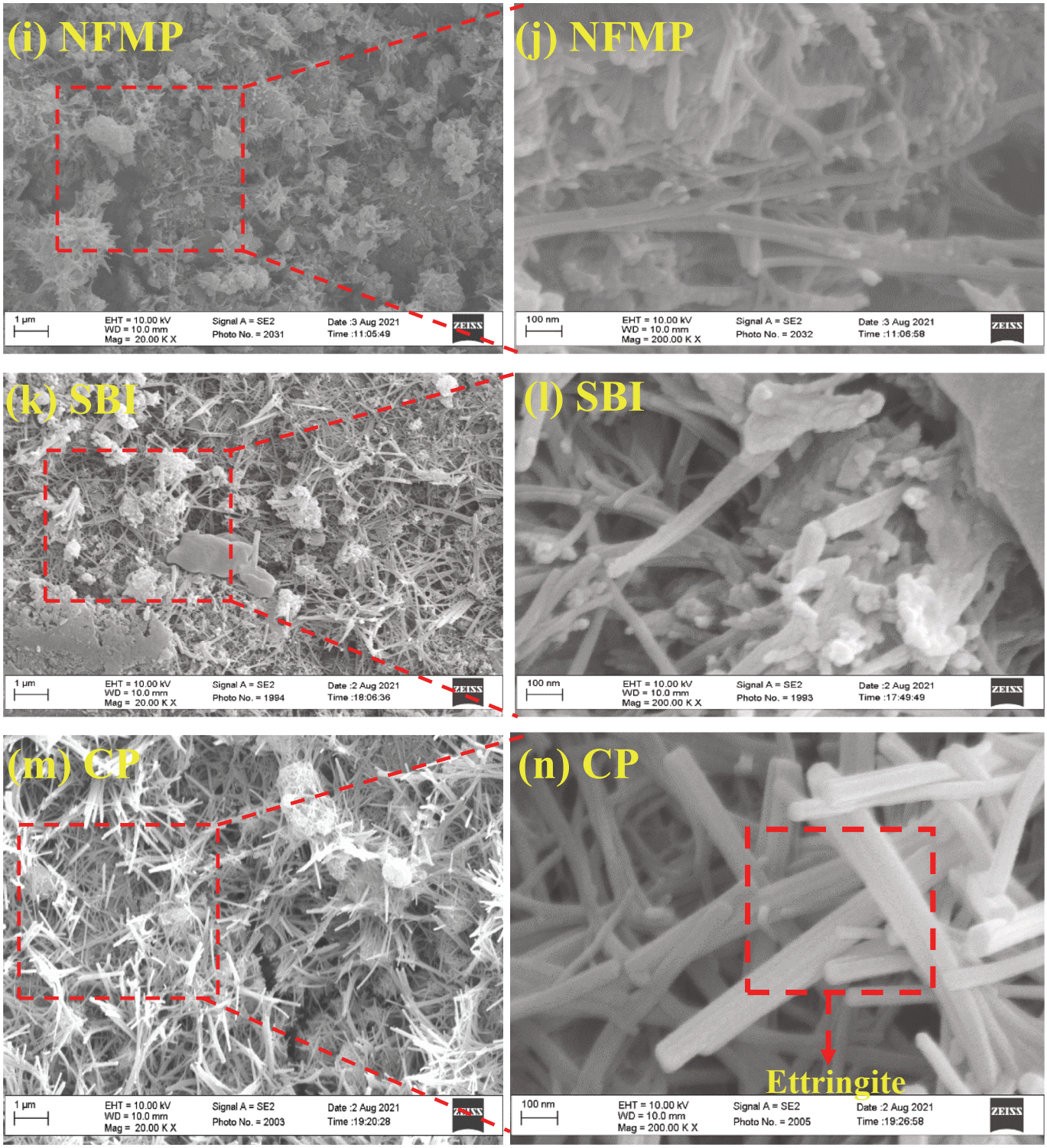

Fig. 10. (*continued*).

respectively are listed in Table 2. It is observed that the samples treated with proteins showed a distinct increase in contact angle, compared to the sample without treatment with proteins. This points to the affinity of the proteins to the cement paste surface. It is noted that the contact angles of the cement paste surfaces generally increased with decreasing surface tension of the protein solutions. This provides an understanding into the relationship between surface tension of the proteins and their ability to induce surface hydrophobicity to cement paste surface.

2.3.8. *Water absorption*

Fig. 12a and b illustrate the water absorption plotted against time for cement paste cured for 3 days and 28 days and treated with and without proteins. It is seen from Fig. 12a that the samples showed a rapid water uptake at the initial stage followed by a gradual increase at later stages. Generally, it can be observed that the water uptake of the control sample was the highest. For instance, the control sample showed a 2.7 % increase in initial mass due to water absorption and subsequently reached an ultimate increment of 11 % at 360 min. In comparison, whey protein,

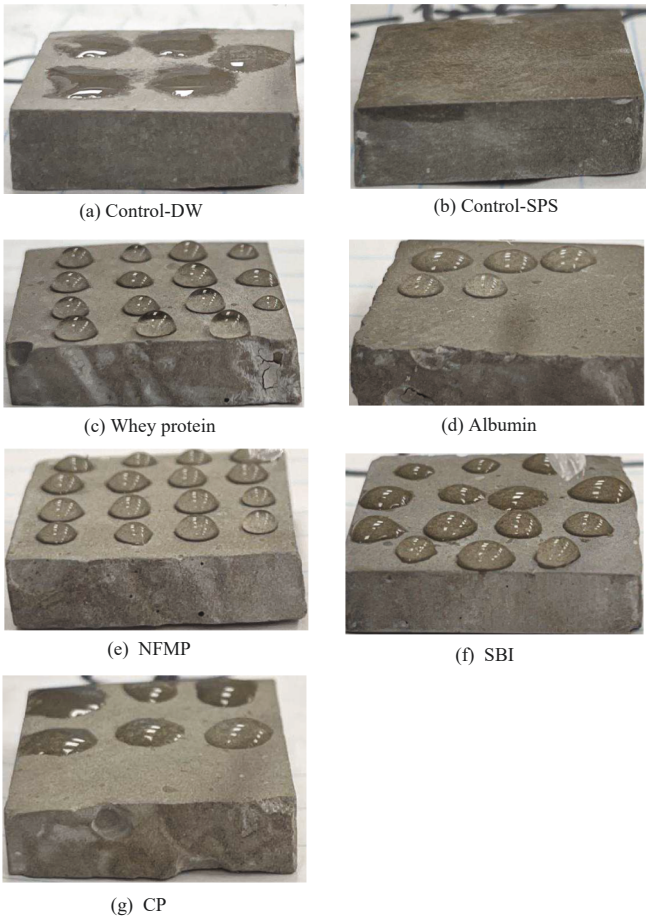

Fig. 11. Photograph illustrating the effect of hydrophobic proteins on the contact angle of cementitious surface.

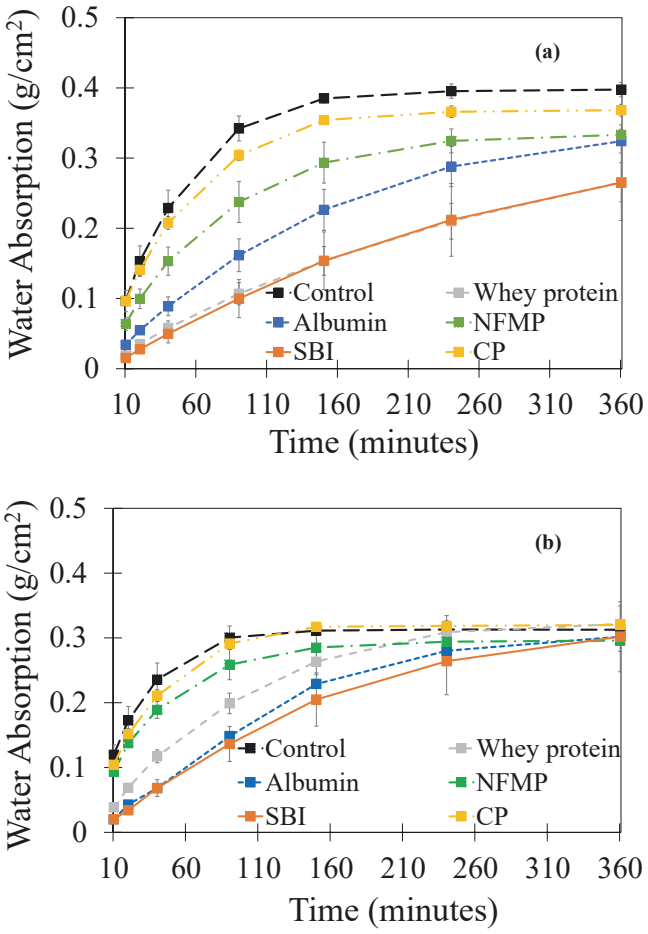

Fig. 12. Water absorption of cement paste samples cured for (a) 3 days and (b) 28 days.

Table 2
Contact angle measurement of treated cementitious surfaces.

Sample	Contact angle (°)	
	7 days	28 days
Control-DW	8	7
Control-SPS	0	0
Whey protein	73.9	74.2
Albumin	49	59
NFMP	47.9	51.1
SBI	46	57
CP	32.5	27

albumin and NFMP treated samples showed initial mass increment of 0.5 %, 0.9 % and 0.44 %, respectively and ultimately reached 7.4 %, 8.8 %, and 7.5 % respectively at 360 min. The mechanism by which proteins influence the water absorption in the cement paste can be explained as follows. Proteins could modify the microstructure on the surface. This was demonstrated in the SEM images where it was shown that the presence of some proteins including whey protein, albumin and SBI resulted in a change in the morphology of ettringite. Among the proteins, CP treated samples exhibited the highest water uptake although their values were still lower than the control. Interestingly, as indicated before, CP showed little modification on the ettringite, and this could be attributed to the weaker adsorption of CP onto the ettringite. Another reason why proteins generally showed lower water absorption could be due to the adsorption of proteins onto the cement paste surface through Ca^{2+} bridging forming a film network on the surface, which could reduce transport of water through the surface. Another important factor which could contribute to the reduced water absorption in some of the protein treated samples is the formation of hydrophobic surfaces due to the adsorption of proteins onto some hydrated phases on the surface, as shown in the FTIR and SEM results. Hydrophobic materials such as proteins and other polymers may induce water repelling effect [82] on the cement and concrete surfaces and that generally lowers the rate at which water is absorbed by the cement paste [57]. It is interesting to note that the water absorption trend follows a similar trend to the protein hydrophobicity as revealed by the surface tension results. For instance, whey protein and SBI which showed the lowest surface tension in SPS exhibited the lowest water uptake while the higher surface tension of CP translated into higher water absorption. Modification of cement microstructure through the formation of hydrophobic surfaces has been observed in prior studies [83,84]. Fig. 12b illustrates the effect of protein treatment on the water absorption of cement paste cured for 28 days. Comparing the control samples in Fig. 12a and b, it is observed that the control sample corresponding to 3-day cured showed higher water absorption than the sample corresponding to 28-day cured. This is attributed to the densification of the microstructure due to the formation of more hydration products [39]. In addition, early age cement paste has been reported to be more hydrophilic than old age cement paste [85]. It is seen in Fig. 12b that, samples cured for 28 days and treated with proteins, specifically the samples with whey protein, albumin and SBI showed reduced water uptake at the initial stages compared to the control sample but their water uptake reached that of the control sample at later stages of the test.

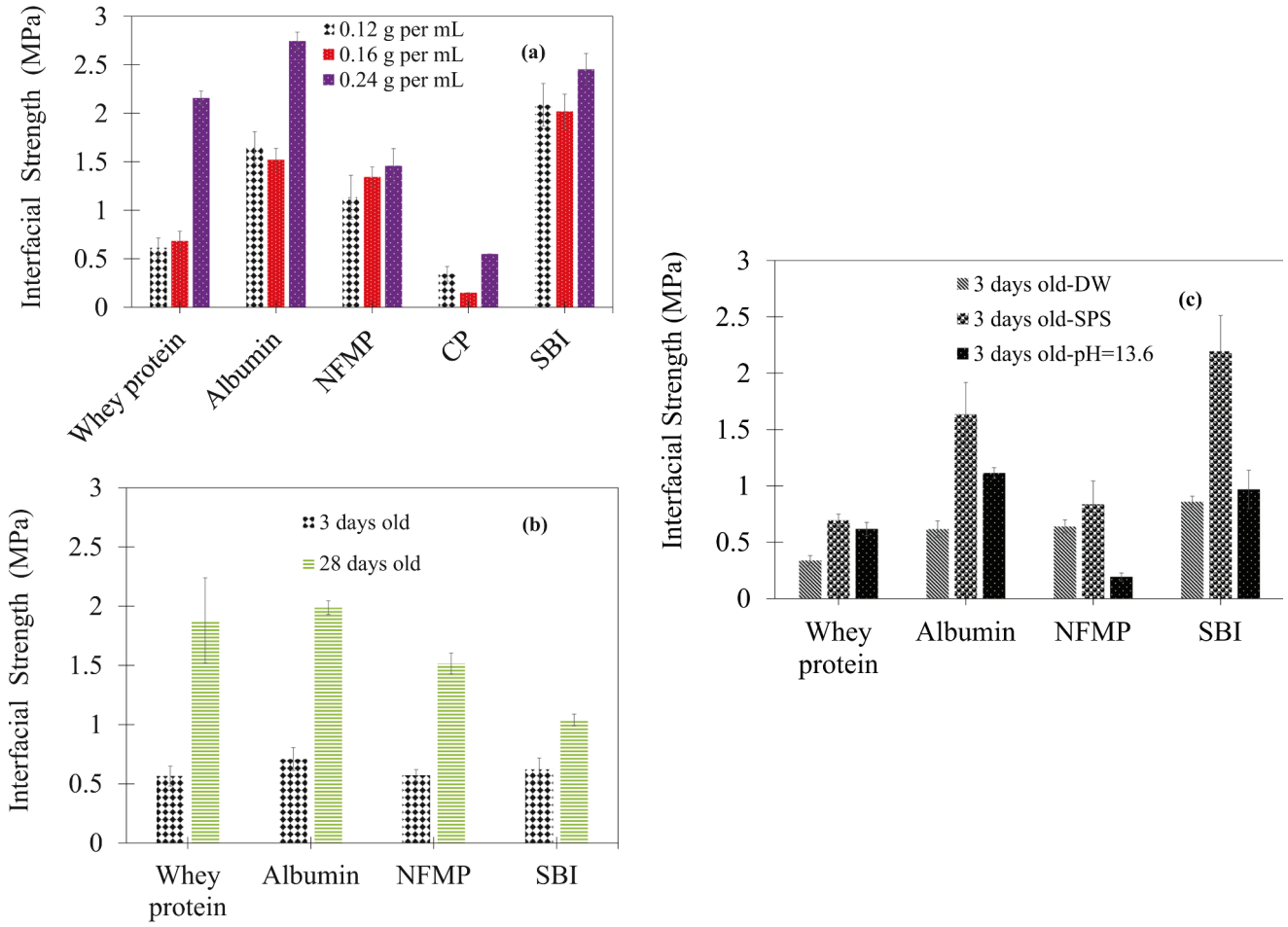

Fig. 13. Interfacial strength of cement paste (a) with respect to protein concentration (b) with respect to the age of cement paste and (c) with respect to different protein solution conditions.

2.3.9. Interfacial strength

The interfacial strength between the proteins and cement paste is illustrated in Fig. 13a–c. From Fig. 13a, it is seen that the interfacial strength between the proteins and the cementitious surface increased with increasing concentration. The observed trend may be attributed to the increased protein viscosity and bond strength as a result of the increased protein concentration. Protein concentration can influence the viscosity of the solution and thickness of the bond formed and, therefore, could have an influence on the interfacial shear strength [86]. Meredith et al. [87] studied the adhesive strength of synthetic mussel-mimetic polymer and observed an increase in adhesive strength when the concentration of the adhesive solution was increased from 0.75 to 1.2 g mL^{-1}. This, they attributed to increased viscosity and bond thickness resulting from the high concentration of the protein solution. It is noted that the effect of concentration on the increased interfacial strength seems to be different among the proteins; in particular, whey protein and albumin exhibited a drastic increase in interfacial strength at the 0.24 g/mL concentration compared to other proteins. Regardless of the concentration, CP treated samples showed lower interfacial strength at all the concentrations. The observed behavior of CP can be attributed to its inability to interact with cement paste surface and form a gel to serve as a bond line. Previous studies have established that adhesive strength of proteins increases with increasing protein molecular weight [22,88]. CP comprises of small molecules with a molecular weight less than 10 k g/mol which is far lower than the other proteins studied here. For instance, the molecular weight of albumin, whey protein, and SBI are 44 k g/mol, 41.7 k g/mol, and 160 k g/mol, respectively while the molecular weight of CP is less than 10 k g/mol [11,89,90]. Lower molecular weight proteins have reduced chain length of amino acid. Prior to the breakage of the CP molecular bond during shear strength test, the amino acids are shortened unlike the proteins with higher molecular weight and long amino acids which may allow elongation prior to breakage [88,91]. The reduced chain length in CP could reduce interfacial strength. In addition, the relatively low viscosity of CP compared to other proteins (data not shown here), inhibited the formation of adhesive layer which eventually weakened the bond strength between the cementitious surface and the protein after the curing process [92].

The pore structure, surface area, surface chemical characteristics, and pore solution properties of cement paste changes with hydration [93]. To investigate the effect of the surface characteristics of the cement paste on the interfacial strength between proteins and cement paste, tests were performed on the cement paste corresponding to 3 days and 28 days of curing (Fig. 13b). It is seen from Fig. 13b that the interfacial strength generally increased with increasing the age of cement paste surface. The interfacial strength arises from the (i) chemical and physical interactions between the proteins and the cement paste surface and (ii) the mechanical interlocking. The mechanical interlocking results from the penetration of the protein adhesive into the asperities of the cement paste surface thus it depends on the surface microstructure. The microstructure of the cement paste becomes more densified with age as hydration continues; thus, it is expected that the cement paste cured for 3 days has more surface porosity and can provide a larger mechanical interlocking compared to the cement paste surface cured for 28 days. However, as seen in Fig. 13b, the interfacial strength of the 3-day cured cement paste is lower than that of the 28-day cured cement paste. Thus, this provides a strong evidence that the physical and chemical molecular

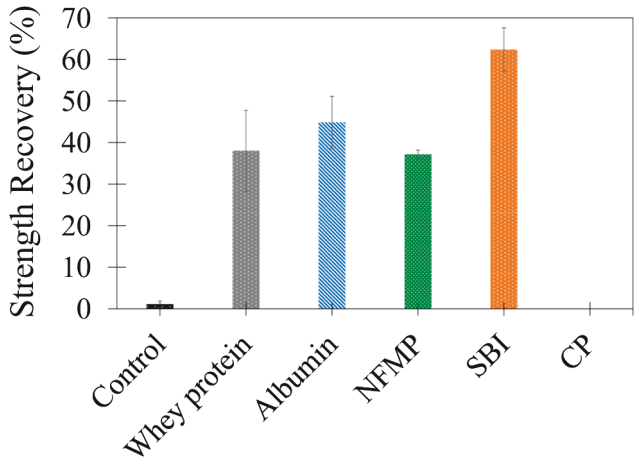

Fig. 14. Strength recovery of healed samples.

bonds between the protein and cement paste surface and the cohesive strength of the protein adhesive are responsible for the increased interfacial strength results shown in Fig. 13b. It is expected that the surface of the 3-day sample consists of more reactive unhydrated cement clinkers compared to the surface of the 28-day sample; thus, the bonds formed between the protein molecules and the surface of reactive cement clinker can be broken as the cement clinker surface continually dissolves into the adjacent solution near the interface.

Protein denaturation in alkaline medium has been observed to influence the adhesive strength of protein molecule. To further investigate the effect of the chemistry of cement on the protein interfacial strength, the interfacial strength of proteins dissolved in alkaline solution and in SPS was determined and compared with the interfacial strength of proteins dissolved in DW. The results are shown in Fig. 13c. It is seen that generally the interfacial strength of the samples with protein dissolved in alkaline solution or SPS showed an increase compared to the sample with proteins dissolved in DW; except in the case of the sample with NFMP dissolved in alkaline solution. The increase in interfacial strength of the proteins dissolved in alkaline solution or SPS is attributed to the increased interaction between the protein and the cement surface due to the denaturation of the protein in the high pH solution. It can also be observed that the samples with proteins dissolved in SPS generally demonstrated a higher interfacial strength than those with proteins dissolved in alkaline solution except in the case of NFMP. The extent of this increase varied among the proteins with SBI showing markedly larger increase compared to the other proteins. A potential explanation for the increased interfacial strength in the samples with proteins dissolved in SPS compared to alkaline solution can be the formation of

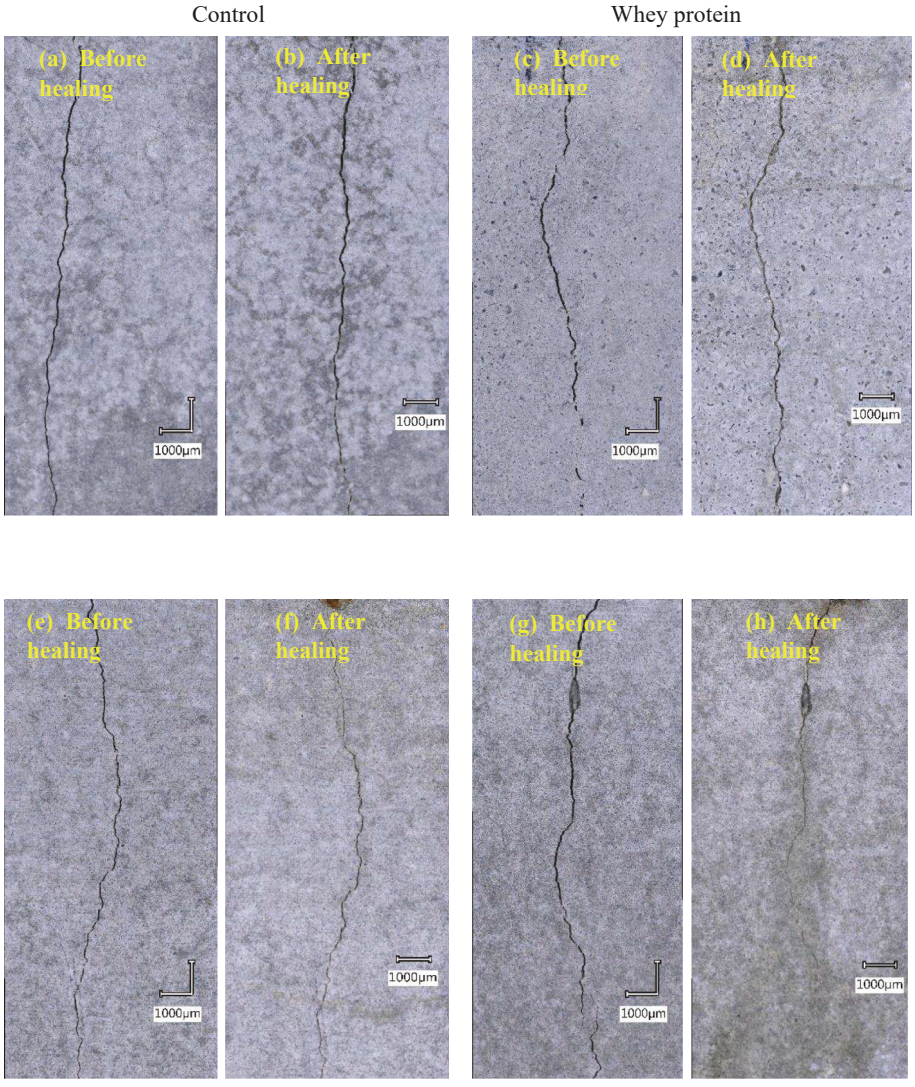

Fig. 15. Crack filling of samples before and after healing.

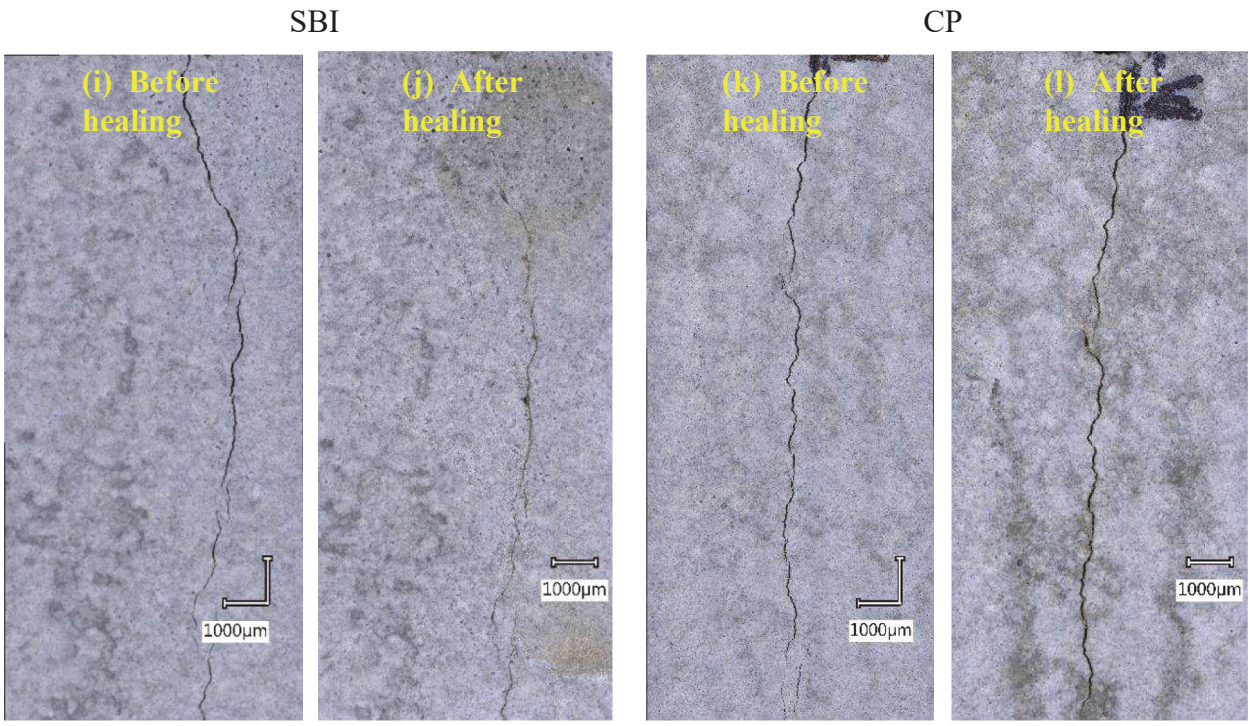

Fig. 15. (*continued*).

crosslink networks due to the presence of ions in the SPS. As discussed, the crosslinking between the negatively charged functional groups of the proteins and the Ca^{2+} is capable of forming a molecular network that could improve the interfacial strength. Generally, it is seen that NFMP dissolved in alkaline solution showed lower interfacial strength compared to when it was dissolved in either DW or in SPS. The observed lower interfacial strength may be attributed to the hydrolyses of the NFMP which results in the breakdown of the peptide bonds and lowering of the molecular weight of NFMP thus, making it less effective in forming a strong adhesive layer during the curing process. It is interesting to note that both albumin and SBI that resulted in higher interfacial strength also demonstrated higher viscosities compared to other proteins studied here (data not shown here). While the underlying mechanisms responsible for the viscosity and interfacial strength are not similar, the higher tendency to self-assemble and form stronger crosslinked networks could contribute to the higher viscosity and interfacial strength of these proteins.

2.3.10. *Flexural strength recovery*

Fig. 14 illustrates the flexural strength recovery of pre-cracked prisms. It is seen that the samples treated in DW only and in the CP solution showed no or significantly lower load recovery compared to the samples treated in the other protein solutions. The insignificant load recovery of the sample treated in CP solution seems to be in agreement with the interfacial strength results discussed in Fig. 13a. Low molecular weight and the inability of the CP to form a bond line to facilitate the adhesion between the cracked surfaces are responsible for the insignificant load recovery of the sample treated in the CP solution. The marginal load recovery exhibited by the control sample may be attributed to autogenous healing as a result of the hydration of the unreacted products and $CaCO_3$ [94]. It is interesting to note the higher load recovery of the sample treated in the SBI solution compared to samples treated in the other protein solutions studied here. This observation was generally in line with the interfacial strength results shown in Fig. 13a and b. Samples healed in whey protein, albumin, and NFMP solutions, and sample healed in the SBI solution showed strength recovery approximately 40 % and 68 % higher than the control sample, respectively. This observation

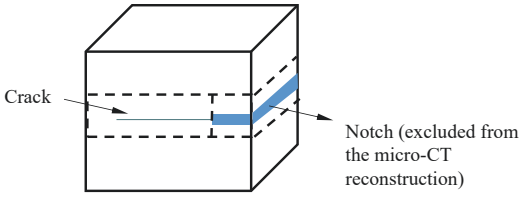

Fig. 16. Schematic showing the section of the prisms used in the micro-CT analysis.

is attributed to the ability of the proteins to bind to the charged cement particle [41] and self-assemble to form a bond line which bonds the cracked surfaces together. It is worth to note from the SEM examination of the sample treated with albumin, SBI and NFMP demonstrated increased modification of the microstructure of the surface product compared to the control sample or the sample treated with CP. Thus, this can also explain the higher strength recovery of the samples treated with these proteins compared to that of the control sample or the sample treated with CP.

2.3.11. *Evaluation of crack filling*

2.3.11.1. Optical imaging. The crack filling ability of the samples treated in the protein solutions could provide an insight into the adsorption of the protein to cement paste surface and their sealing property. The optical images of the various samples before and after treatment are shown in Fig. 15. It is observed that samples healed in protein solutions showed better crack closure ability compared to the samples in DW (Fig. 15b) with the exception of samples healed in CP solution (Fig. 15l). Also, it is noted that the sample healed in SBI (See Fig. 15j) appeared to show the largest filling compared to the samples healed in other protein solutions. It is interesting to note that the crack filling results of the proteins appeared to be in good agreement with the strength recovery results discussed previously. The crack closing ability of the proteins (polymeric adhesive) is in support of earlier observation

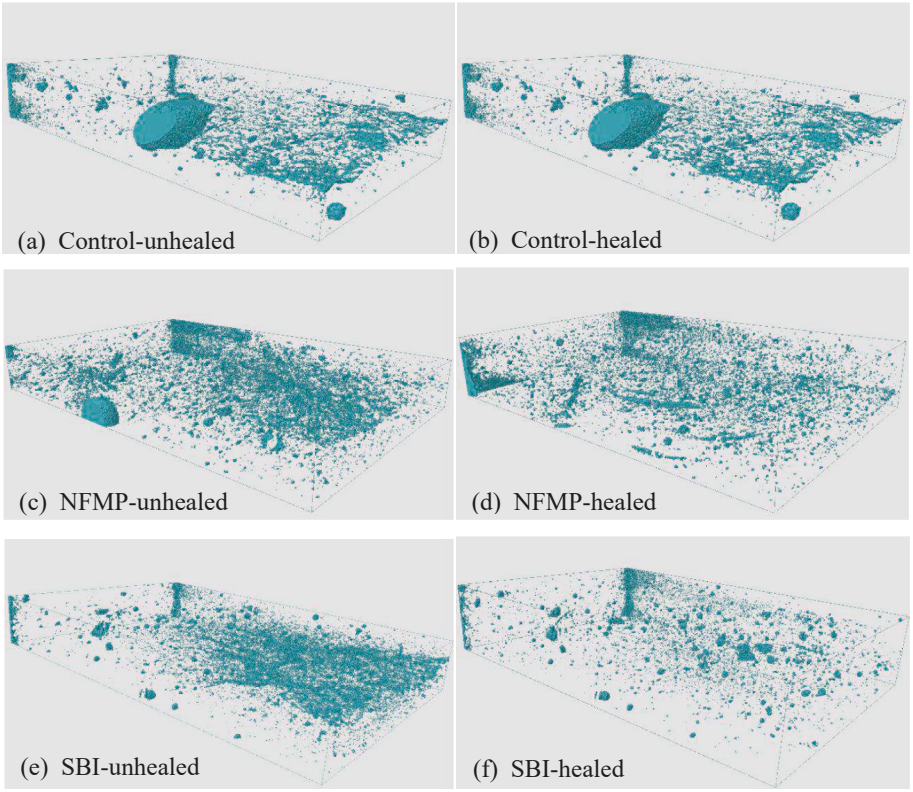

Fig. 17. Micro-CT images of samples illustrating empty space (voids and single crack) (a) before healing and (b) after 14 days of healing. Empty space is shown in turquoise.

made by [95] where it was discovered that polymers have the adhesive property that could seal internally created cracks and bind cracked surfaces together. Depending on the proteins adhesive property, when they adsorb onto the cement particle, they are able to self-assemble to form a gel network that binds the crack surfaces together.

2.3.11.2. X-ray micro-CT imaging. Fig. 16 and Fig. 17 illustrate the section used for the micro-CT analysis and the 3-D reconstruction of the internal microstructure of the samples near the crack before and after treatment, respectively. Empty space including the main crack and voids in the samples are shown in turquoise. Thus, a reduction in the volume of turquoise features can be related to the filling of the crack in the samples. It is noticed that the control sample before and after (Fig. 17a and b) the healing process did not show any variation in in terms of crack filling as the two respective images appear to show a similar total volume of free spaces. This possibly can be attributed to the inefficient autogenous healing process as was observed in the optical images. It can be observed that the samples healed in protein solution showed some improvements in terms of crack filling. As can be observed, the crack in the samples submerged in NFMP solution (Fig. 17d) were slightly healed compared to the sample before healing (Fig. 17c). Interestingly, it can be seen that the SBI healed samples (Fig. 17f) showed the most improved crack filling as demonstrated by the reduced free space near the crack. Thus, the micro-CT results seem to be in a good agreement with the optical imaging results discussed previously.

3. Conclusions

The interaction between five proteins with different molecular structures and a cementitious surface was examined. The findings from this study are as follows:

- The surface charge and hydrodynamic size of the proteins were dependent on pH and this dependence varied among the proteins and was related to the nature of conformation changes occurring in the molecular structure of the proteins. A reduction in the hydrodynamic size of most of the proteins as the pH increased from the native state to the level of pH 13 was observed.
- The surface tension of the protein solutions was shown to be affected by the pH and ionic characteristics of the synthetic pore solution. However, no clear trend on change in surface tension in SPS and DW among the proteins studied here could be established.
- FTIR, TGA, and XRD showed the presence of $CaCO_3$, C—S—H and ettringite in the product formed on the surface of cement paste exposed to ambient air. It was shown that in the samples treated with proteins, the $CaCO_3$ content was generally lower than that in the control samples more likely due to the reduced reaction rate as a result of protein adsorption on the cementitious surface.
- SEM examination of the product formed on the surface of cement paste exposed to ambient air demonstrated different morphology in ettringite between the samples treated with proteins and the control sample. In the samples treated with most of the proteins studied here ettringite seemed to be shorter compared to that in the control sample; in addition, the surface texture of ettringite in the samples treated with certain proteins appeared rougher than in the control sample indicative of protein adsorption on the ettringite and potentially other interactions.
- The contact angle of the samples treated with proteins was shown to be higher than the control sample and the increase in contact angle seemed to be in a general agreement with the reducing effect of the proteins on the solution surface tension.
- It was found that the water absorption of the sample treated with proteins was lower than that of the control sample. The water absorption results appeared to be in a good agreement with the protein

hydrophobicity as determined by the surface tension and contact angle measurements.

- The interfacial strength of the proteins and cementitious surface was shown to be higher for the 28-day sample compared to the 3-day sample; the more reactive nature of the early age sample due to the presence of more unhydrated cement particles on the surface could weaken the bond at the interface. It was shown that the increase in alkalinity and presence of ions in SPS increased the interfacial strength of the proteins. Protein denaturation changes the molecular structure of the proteins and in conjunction with the complexation effect of certain ions including Ca^{2+}, could influence the gelation of the proteins leading to stronger interfacial bond.
- The cracked samples treated with proteins, except CP showed a markedly higher strength recovery compared to the samples treated without proteins. The effect of proteins on the strength recovery was in a good agreement with their effect on the interfacial strength results.
- Optical and X-ray micro-CT imaging showed improved crack filling in the samples treated with proteins compared to the control sample. The crack filling ability of the proteins followed their strength recovery ability with SBI exhibiting the highest and CP the lowest effect.

Declaration of Competing Interest

The authors declare that they have no known competing financial interests or personal relationships that could have appeared to influence the work reported in this paper.

Data availability

Data will be made available on request.

Acknowledgements

This study was supported in part by the National Science Foundation under the CAREER award number 1846984. The X-ray micro-CT imaging was made possible by the National Science Foundation under the MRI award number 1920127.

References

[1] A. Mignon, D. Snoeck, D. Schaubroeck, N. Luickx, P. Dubruel, S. Van Vlierberghe, N. De Belie, PH-responsive superabsorbent polymers: A pathway to self-healing of mortar, React. Funct. Polym. 93 (2015) 68–76.
[2] J. Xu, W. Yao, Multiscale mechanical quantification of self-healing concrete incorporating non-ureolytic bacteria-based healing agent, Cem. Concr. Res. 64 (2014) 1–10.
[3] K. Wang, D.C. Jansen, S.P. Shah, A.F. Karr, Permeability study of cracked concrete, Cem. Concr. Res. 27 (3) (1997) 381–393.
[4] E. Tziviloglou, V. Wiktor, H.M. Jonkers, E. Schlangen, Bacteria-based self-healing concrete to increase liquid tightness of cracks, Constr. Build. Mater. 122 (2016) 118–125.
[5] V. Wiktor, H.M. Jonkers, Quantification of crack-healing in novel bacteria-based self-healing concrete, Cem. Concr. Compos. 33 (7) (2011) 763–770.
[6] A.M. Belcher, X.H. Wu, R.J. Christensen, P.K. Hansma, G.D. Stucky, D.E. Morse, Control of crystal phase switching and orientation by soluble mollusc-shell proteins, Nature. 381 (6577) (1996) 56–58.
[7] J.B. Thompson, G.T. Paloczi, J.H. Kindt, M. Michenfelder, B.L. Smith, G. Stucky, D. E. Morse, P.K. Hansma, Direct observation of the transition from calcite to aragonite growth as induced by abalone shell proteins, Biophys. J. 79 (6) (2000) 3307–3312.
[8] S. Raz, P.C. Hamilton, F.H. Wilt, S. Weiner, L. Addadi, The Transient Phase of Amorphous Calcium Carbonate in Sea Urchin Larval Spicules: The Involvement of Proteins and Magnesium Ions in Its Formation and Stabilization, Adv. Funct. Mater. 13 (2003) 480–486.
[9] S.M. Song, I.H. Kim, Biomineralization of calcium carbonate by adding aspartic acid and lysozyme 28 (2011) 1749–1753.
[10] Y. Liu, Y. Chen, X. Huang, G. Wu, Biomimetic synthesis of calcium carbonate with different morphologies and polymorphs in the presence of bovine serum albumin and soluble starch, Mater. Sci. Eng. C. 79 (2017) 457–464.
[11] X. Wang, R. Kong, X. Pan, H. Xu, D. Xia, H. Shan, J.R. Lu, Role of Ovalbumin in the Stabilization of Metastable Vaterite in Calcium Carbonate Biomineralization, Role of Ovalbumin in the Stabilization of Metastable Vaterite in Calcium Carbonate Biomineralization 113 (26) (2009) 8975–8982.
[12] N. Wu, H.-X. Pan, D. Qiu, Y.-M. Zhang, Feasibility of EPS-producing bacterial inoculation to speed up the sand aggregation in the Gurbantunggut Desert, Northwestern China 54 (12) (2014) 1378–1386.
[13] O.Y.A. Costa, J.M. Raaijmakers, E.E. Kuramae, Microbial extracellular polymeric substances: Ecological function and impact on soil aggregation, Front. Microbiol. 9 (2018) 1–14.
[14] E. Vignaga, H. Haynes, W.T. Sloan, Quantifying the tensile strength of microbial mats grown over noncohesive sediments, Biotechnol. Bioeng. 109 (5) (2012) 1155–1164.
[15] J. Tourney, B.T. Ngwenya, of, Chem. Geol. 386 (2014) 115–132.
[16] H. Rong, C.-X. Qian, Binding functions of microbe cement, Adv. Eng. Mater. 17 (3) (2015) 334–340.
[17] F. Yang, B. Zhang, Q. Ma, Study of sticky rice-lime mortar technology for the restoration of historical masonry construction, Acc. Chem. Res. 43 (6) (2010) 936–944.
[18] W.-Y. Ching, L. Poudel, S. San, K. Baral, Interfacial Interaction between Suolunite Crystal and Silica Binding Peptide for Novel Bioinspired Cement, ACS Comb. Sci. 21 (12) (2019) 794–804.
[19] Z. Zhong, X. Susan Sun, X. Fang, J.A. Ratto, Adhesion properties of soy protein with fiber cardboard, JAOCS, J. Am. Oil Chem. Soc. 78 (1) (2001) 37–41.
[20] K. Li, S. Peshkova, X. Geng, Investigation of soy protein-kymene® adhesive systems for wood composites, JAOCS, J. Am. Oil Chem. Soc. 81 (5) (2004) 487–491.
[21] J.K. Román, J.J. Wilker, Cooking Chemistry Transforms Proteins into High-Strength Adhesives, J. Am. Chem. Soc. 141 (3) (2019) 1359–1365.
[22] M.J. Brennan, S.E. Hollingshead, J.J. Wilker, J.C. Liu, Critical factors for the bulk adhesion of engineered elastomeric proteins, R. Soc. Open Sci. 5 (5) (2018) 171225.
[23] I. Santoni, B. Pizzo, Evaluation of alternative vegetable proteins as wood adhesives, Ind. Crops Prod. 45 (2013) 148–154.
[24] N.D.V. Raydan, L. Leroyer, B. Charrier, E. Robles, Recent advances on the development of protein-based adhesives for wood composite materials—a review, Molecules. 26 (24) (2021) 7617.
[25] L. Ventol, M. Vendrell, P. Giraldez, L. Merino, Traditional organic additives improve lime mortars: New old materials for restoration and building natural stone fabrics, Constr. Build. Mater. 25 (2011) 3313–3318.
[26] P. Brzyski, Z. Suchorab, G. Łagód, The influence of casein protein admixture on pore size distribution and mechanical properties of lime-metakaolin paste, Buildings. 11 (11) (2021) 530.
[27] M. Kamali, A. Ghahremaninezhad, Effect of Biomolecules on the Nanostructure and Nanomechanical Property of Calcium-Silicate-Hydrate, Sci. Rep. 8 (2018) 1–16.
[28] T. Chlayon, M. Iwanami, N. Chijiwa, Combined protective action of barnacles and biofilm on concrete surface in intertidal areas, Constr. Build. Mater. 179 (2018) 477–487.
[29] J. Lv, J. Mao, H. Ba, Influence of marine microorganisms on the permeability and microstructure of mortar, Constr. Build. Mater. 77 (2015) 33–40.
[30] J.A. Rosewitz, S. Wang, S.F. Scarlata, N. Rahbar, An enzymatic self-healing cementitious material, Appl. Mater. Today. 23 (2021), 101035.
[31] X. Wang, Z. He, M. Zeng, F. Qin, B. Adhikari, J. Chen, Effects of the size and content of protein aggregates on the rheological and structural properties of soy protein isolate emulsion gels induced by CaSO4, Food Chem. 221 (2017) 130–138.
[32] T.V. Arriaga, Controlled and tailored denaturation and aggregation of whey proteins Tatiana Vieira Arriaga Engenharia Biológica Júri, Thesis. (2011).
[33] M.D. Shoulders, R.T. Raines, Collagen structure and stability, Annu. Rev. Biochem. 78 (1) (2009) 929–958.
[34] M. Singh, Structural interactions of globular proteins – Bovine serum albumin, egg albumin, and lysozyme, in aqueous medium, elucidated with molar volumes, viscosities, energy functions, and IR spectra from 293.15 to 303.15 K, J. Appl. Polym. Sci. 103 (3) (2007) 1420–1429.
[35] N.S. Utay, D.M. Asmuth, S. Gharakhanian, M. Contreras, C.D. Warner, C.J. Detzel, Potential use of serum-derived bovine immunoglobulin/protein isolate for the management of COVID-19, Drug Dev. Res. 1–7 (2021).
[36] D. Barbano, Milk Protein Products – What Are They and What Role Do They Play in Lactose Reduced (Low " Carb ") Foods ? Low " Carb " Dairy Foods and Ingredients, in: Are Milk Protein Products Safe ? Milk components and separation processes, 2009, pp. 1–5.
[37] M.H. Abd El-Salam, S. El-Shibiny, Natural biopolymers as nanocarriers for bioactive ingredients used in food industries, Elsevier Inc., 2016.
[38] J. Delaveau, P. Jelen, Effect of pH on Viscosity of Sweet and Acid Wheys, J. Dairy Sci. 62 (9) (1979) 1455–1457.
[39] N.K. Ilango, P. Gujar, A.K. Nagesh, A. Alex, P. Ghosh, Interfacial adhesion mechanism between organic polymer coating and hydrating cement paste, Cem. Concr. Compos. 115 (2021) 103856.
[40] H. Bian, Colloidal behavior of casein biopolymer in alkaline solution and its application in self-levelling underlayments (SLUs), (2012).
[41] E. Baffoe, A. Ghahremaninezhad, The effect of biomolecules on enzyme-induced calcium carbonate precipitation in cementitious materials, Constr. Build. Mater. 345 (2022), 128323.
[42] H. Bian, J. Plank, Re-association behavior of casein submicelles in highly alkaline environments, Zeitschrift Fur Naturforsch. – Sect. B J. Chem. Sci. 67 (2012) 621–630.
[43] J.F. Schmitz, Enzyme modified soy flour adhesives, (2009).
[44] J. Li, C. Wang, X. Li, Y. Su, Y. Yang, X. Yu, Effects of pH and NaCl on the physicochemical and interfacial properties of egg white/yolk, Food Biosci. 23 (2018) 115–120.

[45] A. Kato, S. Nakai, Hydrophobicity determined by a fluorescence probe method and its correlation with surface properties of proteins, Biochim. Biophys. Acta. 624 (1) (1980) 13–20.
[46] H. Xiao, L. Huang, W. Zhang, Z. Yin, Damage of proteins at the air/water interface: Surface tension characterizes globulin interface stability, Int. J. Pharm. 584 (2020), 119445.
[47] E. Zecca, Investigating the Role of Surface Hydrophobicity in Protein Aggregation, (2017). https://opencommons.uconn.edu/dissertations/1488.
[48] A. Laligant, E. Dumay, C.C. Valencia, J.L. Cuq, J.C. Cheftel, Surface Hydrophobicity and Aggregation of β-Lactoglobulin Heated near Neutral pH, J. Agric. Food Chem. 39 (1991) 2147–2155.
[49] Q. Liu, R. Geng, J. Zhao, Q. Chen, B. Kong, Structural and Gel Textural Properties of Soy Protein Isolate When Subjected to Extreme Acid pH-Shifting and Mild Heating Processes, J. Agric. Food Chem. 63 (19) (2015) 4853–4861.
[50] K.A. Dill, S.B. Ozkan, M.S. Shell, T.R. Weikl, The protein folding problem, Annu. Rev. Biophys. 37 (1) (2008) 289–316.
[51] E. Tatsumi, D. Yoshimatsu, M. Hirose, Conformational state of ovalbumin at acidic pH as evaluated by a novel approach utilizing intrachain sulfhydryl-mixed disulfide exchange reactions, Biochemistry. 37 (35) (1998) 12351–12359.
[52] A. Brüning, J. Jückstock, Misfolded proteins: From little villains to little helpers in the fight against cancer, Front, Oncol. 5 (2015) 1–12.
[53] C. Nick Pace, J. Martin Scholtz, G.R. Grimsley, Forces stabilizing proteins, FEBS Lett. 588 (2014) 2177–2184.
[54] G.J. Lesser, G.D. Rose, Hydrophobicity of amino acid subgroups in proteins, Proteins Struct. Funct. Bioinforma. 8 (1) (1990) 6–13.
[55] A.M. Master, M.E. Rodriguez, M.E. Kenney, N.L. Oleinick, A.S. Gupta, Delivery of the photosensitizer Pc 4 in PEG–PCL micelles for in vitro PDT studies, J. Pharm. Sci. 99 (5) (2010) 2386–2398.
[56] X. Shen, X. Mo, R. Moore, S.J. Frazier, T. Iwamoto, J.M. Tomich, X.S. Sun, Adhesion and structure properties of protein nanomaterials containing hydrophobic and charged amino acids, J. Nanosci. Nanotechnol. 6 (3) (2006) 837–844.
[57] N.S. Hettiarachchy, U. Kalapathy, D.J. Myers, Alkali-modified soy protein with improved adhesive and hydrophobic properties, J. Am. Oil Chem. Soc. 72 (12) (1995) 1461–1464.
[58] A.H. Delgado, R.M. Paroli, J.J. Beaudoin, Comparison of IR techniques for the characterization of construction cement minerals and hydrated products, Appl. Spectrosc. 50 (8) (1996) 970–976.
[59] R. Ylmén, U. Jäglid, B.-M. Steenari, I. Panas, Early hydration and setting of Portland cement monitored by IR, SEM and Vicat techniques, Cem. Concr. Res. 39 (5) (2009) 433–439.
[60] C.E. Weir, E.R. Lippincott, Infrared studies of aragonite, calcite, and vaterite type structures in the borates, carbonates, and nitrates, J. Res. Natl. Bur. Stand. Sect. A Phys. Chem. 65A (3) (1961) 173.
[61] M.Y.A. Mollah, W. Yu, R. Schennach, D.L. Cocke, Fourier transform infrared spectroscopic investigation of the early hydration of Portland cement and the influence of sodium lignosulfonate, Cem. Concr. Res. 30 (2000) 267–273.
[62] M. Thiery, G. Villain, P. Dangla, G. Platret, Investigation of the carbonation front shape on cementitious materials: Effects of the chemical kinetics, Cem. Concr. Res. 37 (7) (2007) 1047–1058.
[63] R. Ylmén, L. Wadsö, I. Panas, Insights into early hydration of Portland limestone cement from infrared spectroscopy and isothermal calorimetry, Cem. Concr. Res. 40 (10) (2010) 1541–1546.
[64] T.L. Hughes, C.M. Methven, T.G.J. Jones, S.E. Pelham, P. Fletcher, C. Hall, Determining cement composition by Fourier transform infrared spectroscopy, Adv. Cem. Based Mater. 2 (3) (1995) 91–104.
[65] J.T. Kloprogge, R.D. Schuiling, Z. Ding, L. Hickey, D. Wharton, R.L. Frost, Vibrational spectroscopic study of syngenite formed during the treatment of liquid manure with sulphuric acid, Vib. Spectrosc. 28 (2) (2002) 209–221.
[66] S. Lamberet Durability of ternary binders based on portland cement, calcium aluminate cement and calcium sulfate, PhD thesis N°3151 Ecole Polytechnique Fédérale de Lausanne 3151 (2005).
[67] T. Vázquez-Moreno, M.T. Blanco-Varela, Tabla de frecuencias y espectros de absorción infrarroja de compuestos relacionados con la química del cemento, Mater. Construcción. 31 (182) (1981) 31–48.
[68] C. Valenzuela, L. Abugoch, C. Tapia, A. Gamboa, Effect of alkaline extraction on the structure of the protein of quinoa (Chenopodium quinoa Willd.) and its influence on film formation, Int. J. Food Sci. Technol. 48 (4) (2013) 843–849.
[69] W. Gallagher, FTIR Analysis of Protein Structure (1997) 662–666.
[70] R.I. Khan, W. Ashraf, J. Olek, Amino acids as performance-controlling additives in carbonation-activated cementitious materials, Cem. Concr. Res. 147 (2021) 106501.
[71] D.A. Silva, H.R. Roman, P.J.P. Gleize, Evidences of chemical interaction between EVA and hydrating Portland cement, Cem. Concr. Res. 32 (9) (2002) 1383–1390.
[72] M. Zhang, J. Shen, R. Yang, H. Ji, J. Ding, Effect of Curing Age on the Microstructure and Hydration Behavior of Oil Well Cement Paste Cured at High Temperature, J. Mater. Civ. Eng. 33 (2021) 04021006.
[73] M. Yáñez, J. Gil-Longo, M. Campos-Toimil, Calcium binding proteins, Adv. Exp. Med. Biol. 740 (2012) 461–482.
[74] W. Liu, Y.Q. Li, L.P. Tang, Z.J. Dong, XRD and 29Si MAS NMR study on carbonated cement paste under accelerated carbonation using different concentration of CO2, Mater. Today Commun. 19 (2019) 464–470.
[75] V. Rostami, Y. Shao, A.J. Boyd, Z. He, Microstructure of cement paste subject to early carbonation curing, Cem. Concr. Res. 42 (1) (2012) 186–193.
[76] D. Sharma, S. Goyal, Accelerated carbonation curing of cement mortars containing cement kiln dust: An effective way of CO2 sequestration and carbon footprint reduction, J. Clean. Prod. 192 (2018) 844–854.
[77] M. Auroy, S. Poyet, P. Le Bescop, J.M. Torrenti, T. Charpentier, M. Moskura, X. Bourbon, Comparison between natural and accelerated carbonation (3% CO2): Impact on mineralogy, microstructure, water retention and cracking, Cem. Concr. Res. 109 (2018) 64–80.
[78] P.E. Stutzman Scanning Electron Microscopy in Concrete Petrography Mater. Sci. Concr. Spec. 2001 59 72 http://fire.nist.gov/bfrlpubs/build01/PDF/b01086.pdf.
[79] M. Liu, Y. Gao, L. Zhang, G. Jiang, C. Zeng, P. Wang, The application of thermal analysis to study the hydration behavior of tricalcium aluminate-gypsum in the presence of polycarboxylate-based superplasticizers, Thermochim. Acta. 696 (2021), 178821.
[80] J. Plank, D. Zhimin, H. Keller, F.v. Hössle, W. Seidl, Fundamental mechanisms for polycarboxylate intercalation into C3A hydrate phases and the role of sulfate present in cement, Cem. Concr. Res. 40 (1) (2010) 45–57.
[81] J. Plank, C. Hirsch, Impact of zeta potential of early cement hydration phases on superplasticizer adsorption, Cem. Concr. Res. 37 (4) (2007) 537–542.
[82] W. Huang, X. Sun, Adhesive properties of soy proteins modified by urea and guanidine hydrochloride, JAOCS, J. Am. Oil Chem. Soc. 77 (1) (2000) 101–104.
[83] P. Liu, C. Feng, F. Wang, Y. Gao, J. Yang, W. Zhang, L.u. Yang, Hydrophobic and water-resisting behavior of Portland cement incorporated by oleic acid modified fly ash, Mater. Struct. Constr. 51 (2) (2018).
[84] H.S. Wong, R. Barakat, A. Alhilali, M. Saleh, C.R. Cheeseman, Hydrophobic concrete using waste paper sludge ash, Cem. Concr. Res. 70 (2015) 9–20.
[85] P. Gujar, A. Alex, M. Santhanam, P. Ghosh, Evaluation of interfacial strength between hydrating cement paste and epoxy coating, Constr. Build. Mater. 279 (2021), 122511.
[86] Adhesives and sealants (2001).
[87] H.J. Meredith, C.L. Jenkins, J.J. Wilker, Enhancing the adhesion of a biomimetic polymer yields performance rivaling commercial glues, Adv. Funct. Mater. 24 (21) (2014) 3259–3267.
[88] A. Galliano, S. Bistac, J. Schultz, Adhesion and friction of PDMS networks: Molecular weight effects, J. Colloid Interface Sci. 265 (2) (2003) 372–379.
[89] M. Schmid, S. Pröls, D.M. Kainz, F. Hammann, A. Stäbler, Impact of Hydrolyzed Whey Protein on the Molecular Interactions and Cross-Linking Density in Whey Protein Isolate-Based Films, Int. J. Polym. Sci. 2016 (2016) 1–9.
[90] A. Le, A. Morales-peñaloza, M. Mart, Hydrolyzed Collagen—Sources and Applications, (n.d.) 1–16.
[91] C.L. Jenkins, H.J. Meredith, J.J. Wilker, Molecular weight effects upon the adhesive bonding of a mussel mimetic polymer, ACS Appl. Mater. Interfaces. 5 (11) (2013) 5091–5096.
[92] C. Liu, Y. Zhang, X. Li, J. Luo, Q. Gao, J. Li, "Green" bio-thermoset resins derived from soy protein isolate and condensed tannins, Ind. Crops Prod. 108 (2017) 363–370.
[93] H.F.W. Taylor, Cement chemistry, Cem, Chem, 1997.
[94] G. Lefever, D. Snoeck, D.G. Aggelis, N. De Belie, S. Van Vlierberghe, D. Van Hemelrijck, Evaluation of the self-healing ability of mortar mixtures containing superabsorbent polymers and nanosilica, Materials (Basel). 13 (2) (2020) 380.
[95] F.A. Gilabert, K. Van Tittelboom, J. Van Stappen, V. Cnudde, N. De Belie, W. Van Paepegem, Integral procedure to assess crack filling and mechanical contribution of polymer-based healing agent in encapsulation-based self-healing concrete, Cem. Concr. Compos. 77 (2017) 68–80.